

Original Article

Cite this article: Dong C, Xu Z, Wilde SA, Ma M, Liu S, Xie S, Li P, and Wan Y (2023) Establishing the occurrence of late Neoarchaean – earliest Palaeoproterozoic magmatism in the Daqingshan area, northwestern North China Craton: SIMS U–Pb zircon dating, Lu–Hf and Sm–Nd isotopes and whole-rock geochemistry. *Geological Magazine* **160**: 732–754. <https://doi.org/10.1017/S0016756822001212>

Received: 22 July 2022

Revised: 7 November 2022

Accepted: 22 November 2022

First published online: 3 January 2023

Keywords:

late Neoarchaean; magmatism; Daqingshan; North China Craton; tectonothermal event

Authors for correspondence:


Chunyan Dong,

Email: dongchunyan@sina.com;

Yusheng Wan,

Email: wanyusheng@bjshrmp.cn

Establishing the occurrence of late Neoarchaean – earliest Palaeoproterozoic magmatism in the Daqingshan area, northwestern North China Craton: SIMS U–Pb zircon dating, Lu–Hf and Sm–Nd isotopes and whole-rock geochemistry

Chunyan Dong¹, Zhongyuan Xu², Simon A. Wilde^{1,3}, Mingzhu Ma¹, Shoujie Liu¹, Shiwen Xie¹, Pengchuan Li¹ and Yusheng Wan¹ 

¹Beijing SHRIMP Centre, Institute of Geology, Chinese Academy of Geological Sciences, Beijing 100037, China;

²College of Earth Science, Jilin University, Changchun 130061, China and ³Department of Applied Geology, Curtin University, GPO Box U1987, Perth 6854, WA, Australia

Abstract

Daqingshan is located in the northwestern North China Craton where late Neoarchaean supracrustal rocks occur widely, but where magmatic zircon ages have rarely been reported for plutonic rocks. In this study, we report SIMS U–Pb zircon ages and Hf isotope, whole-rock element and Nd isotope compositions for 12 magmatic samples, including TTG, quartz monzonitic and monzogranitic gneisses, and meta-gabbroic and dioritic rocks. They have magmatic zircon ages of 2530–2469 Ma; some samples have ages of <2.48 Ga likely influenced by late Palaeoproterozoic tectonothermal events, making their ages less reliable. TTG gneisses have low Sr/Y and La/Yb ratios, with whole-rock $\epsilon_{Nd}(t)$ and *in situ* magmatic zircon $\epsilon_{Hf}(t)$ values of +1.2 to +2.4 and –1.1 to +6.2, respectively. Quartz monzonite and monzogranite gneisses and gabbroic to dioritic rocks have similar Nd–Hf isotope compositions to the TTG gneisses. The absence of zircon >2.6 Ga in the early Precambrian rocks suggests that the Sanggan Group may have formed in an oceanic environment, whereas the TTG rocks formed as a result of partial melting of the basaltic rocks of the Sanggan Group under relatively low-pressure conditions. Combined with previous studies, the main conclusions are that in the Daqingshan area, late Neoarchaean magmatism was widespread, the late Mesoarchaean – early Neoarchaean was an important period of juvenile continental crustal growth, and the late Neoarchaean supracrustal and plutonic rocks most likely formed in an arc environment. These are common signatures for Neoarchaean crustal evolution throughout much of the North China Craton, and also globally.

1. Introduction

The formation and evolution of continental crust in the Archaean Eon is a long-term theme of geoscience and is largely related to the genesis of the tonalite–trondhjemite–granodiorite (TTG) suite (e.g. Moyen, 2011; Zhai & Santosh, 2011). As with many cratons worldwide, the North China Craton (NCC) has an early Precambrian basement composed of Archaean blocks and Palaeoproterozoic orogenic belts (Zhao *et al.* 2005; Zhai & Santosh, 2011). In the NCC, the Archaean blocks are mainly composed of late Neoarchaean rocks, but early Neoarchaean magmatism was widely developed, and 4.08–4.0 Ga zircons with magmatic zoning have been discovered; thus, the NCC must have a Hadean geological history (Liu *et al.* 1992; Wan *et al.* 2015, 2021). Commonly, in the late Neoarchaean of the NCC, supracrustal rocks were first deposited and then intruded by TTG at the same time or slightly later, followed closely by metamorphism, anatexis and formation of crustally derived granites (Zhai & Santosh, 2011; Wan *et al.* 2015, 2021). In areas lacking in a late Palaeoproterozoic tectonothermal overprint, rocks older than 2.53–2.52 Ga are commonly affected by strong metamorphism and deformation, whereas younger ones are partially or only weakly metamorphosed and deformed (Wan *et al.* 2015; Li *et al.* 2022). The phenomena became more complicated in the areas that experienced tectonothermal events in late Palaeoproterozoic time, with late Neoarchaean and late Palaeoproterozoic tectonothermal events varying in intensity in different areas from being very strong to very weak (Wan *et al.* 2020).

Daqingshan is a typical area in the northwestern part of the NCC that underwent strong tectonothermal events in both late Neoarchaean and late Palaeoproterozoic times

(Ma *et al.* 2012; Dong *et al.* 2013; Wan *et al.* 2013; Cai *et al.* 2014; Liu, P. H. *et al.* 2017). Here, late Neoproterozoic supracrustal rocks are widely distributed, but there is currently a lack of precise ages on the late Neoproterozoic plutonic rocks. For example, it has been considered that TTG magmatism occurred in early Palaeoproterozoic time (~2.45 Ga), rather than in late Neoproterozoic time (Liu, J. H. *et al.* 2013, 2017), being different from many other areas of the NCC where the majority of magmatism occurred in late Neoproterozoic time rather than early Palaeoproterozoic time (Zhai & Santosh, 2011; Wan *et al.* 2015).

With this controversy in mind, we carried out zircon dating, Hf isotope analysis and whole-rock element and Nd isotopic studies on 12 samples of different plutonic rock types, including TTG gneiss, quartz monzonite gneiss, monzogranite gneiss, meta-gabbro and meta-diorite, to provide new constraints on the timing of Precambrian magmatism and metamorphism in the Daqingshan area and to evaluate the important issues relating to Neoproterozoic crust formation and its evolution.

2. Geological background

The Precambrian metamorphic basement in the Daqingshan area is composed of supracrustal and plutonic rocks of different types and ages (Jin *et al.* 1991, 1992; Xu *et al.* 2002, 2005, 2007; Yang *et al.* 2003, 2006). The supracrustal rocks were divided into the late Neoproterozoic Sanggan Group, the late Neoproterozoic Daqingshan Supracrustal Rocks, the early Palaeoproterozoic Lower Wulashan Group and the late Palaeoproterozoic Upper Wulashan Group (Fig. 1). The Sanggan Group is metamorphosed at upper-amphibolite to granulite facies, with local amphibolite-facies retrogression. It was subdivided into mesocratic and leucocratic granulite units, with their protoliths interpreted as basic-intermediate and intermediate-acid volcano-sedimentary rocks, respectively. Recent secondary ion mass spectrometry (SIMS) zircon dating work has indicated that the formation age of the Sanggan Group is actually 2.55–2.50 Ga (Wan *et al.* 2009; Ma *et al.* 2012), much younger than previously thought (Palaeoproterozoic) mainly based on its strong metamorphism and deformation (Yang *et al.* 2003, 2006). The protolith of the Lower Wulashan Group is similar to the Sanggan Group, and also underwent upper-amphibolite to granulite-facies metamorphism. In early studies, it was considered that the Lower Wulashan Group formed in Archaean time, but in fact, it formed in early Palaeoproterozoic time according to recent SIMS zircon dating (2455–2382 Ma; Dong *et al.* 2022). The Upper Wulashan Group is mainly composed of meta-argillo-arenaceous rocks, calcisilicates, marbles and a small amount of metamorphosed basic rocks. It underwent upper-amphibolite to granulite-facies metamorphism. According to the rock assemblage, the Upper Wulashan Group can be further divided into three lithostratigraphic subunits: garnet-biotite gneiss, diopside gneiss and marble subunits (Xu *et al.* 2002, 2007; Yang *et al.* 2003). Their formation age is late Palaeoproterozoic (2.15–1.95 Ga; Wan *et al.* 2009; Dong *et al.* 2013). The Daqingshan Supracrustal Rocks are similar to the garnet-biotite gneiss subunit of the Upper Wulashan Group, but they contain no graphite, instead, banded iron formation (BIF) is abundant (Dong *et al.* 2014). Dong *et al.* (2014) were the first to separate the Daqingshan Supracrustal Rocks from the garnet-biotite gneiss subunit of the Upper Wulashan Group, and they considered that the rocks formed in early Palaeoproterozoic time mainly based on SIMS zircon dating, which yielded detrital zircon ages of 2.55–2.50 Ga and metamorphic zircon ages of 2.45–2.40 Ga. However,

2.5 Ga meta-diorite intruding the Daqingshan Supracrustal Rocks indicates that they were more likely formed in late Neoproterozoic time (Zhang *et al.* 2016).

Early Precambrian plutonic rocks are also widely distributed in the Daqingshan area, including hypersthene-quartz dioritic and charnockitic gneiss (Shanheyuan gneiss), quartz dioritic-granitic gneiss (Kundulun–Zaoergou gneiss), granitic augen gneiss (Lijiazhi gneiss) and garnet granite gneiss (Hademengou gneiss) (Fig. 1; Xu *et al.* 2002, 2005, 2007; Yang *et al.* 2003, 2006). Some felsic rocks in the Sanggan and Lower and Upper Wulashan groups are possibly TTG rocks overprinted by strong metamorphism, deformation and anatexis (e.g. Wan *et al.* 2009). The Shanheyuan gneiss is dominated by hypersthene-biotite-plagioclase granite gneiss, hypersthene-biotite granodiorite gneiss and hypersthene-biotite monzogranite gneiss, with some hornblende-hypersthene-quartz diorite gneiss and biotite-hornblende-hypersthene-plagioclase granitic gneiss. Granulite and BIF enclaves of different sizes are scattered throughout the Shanheyuan gneiss. The Kundulun–Zaoergou gneiss is mainly composed of quartz diorite–granodiorite gneiss. Gneissic structure is developed in weakly deformed rocks, but banded or striped structures occur where there has been anatexis and stronger deformation. The Lijiazhi gneiss is characterized by its flesh-red appearance, originally containing abundant microcline phenocrysts and now having an augen texture. It also contains Shanheyuan gneiss enclaves. The Hademengou gneiss is only distributed in the Hademengou area, and is of a small scale. It is characterized by garnet and is spatially associated with the Daqingshan Supracrustal Rocks. Using the SIMS U–Pb dating method, Xu *et al.* (2015) obtained apparent ages of 2.49–2.48 Ga for ‘magmatic’ zircons from the Shanheyuan and Kundulun–Zaoergou gneisses to the south of Shiguai. It is considered that the slightly younger ages are due to overprinting by late Neoproterozoic and late Palaeoproterozoic tectonothermal events, although the zircon domains still show magmatic zoning; thus, the TTG rocks more likely formed at the end of the Neoproterozoic period. Using the laser ablation inductively coupled plasma mass spectrometry (LA-ICP-MS) U–Pb dating method, J. H. Liu *et al.* (2013, 2017) obtained apparent ages of ~2.45 Ga for magmatic zircons from TTG and crustally derived granite from the Shanheyuan and Kundulun–Zaoergou gneisses, and thus considered them to be early Palaeoproterozoic in age.

Two episodes of upper-amphibolite to granulite-facies metamorphism have been well documented in the area: in the late Neoproterozoic – early Palaeoproterozoic (2.52–2.45 Ga) and in the late Palaeoproterozoic (1.95–1.80 Ga) (Wan *et al.* 2009; Ma *et al.* 2012; Dong *et al.* 2013, 2014; Liu, P. H. *et al.* 2017; Shi *et al.* 2021). Some zircons with metamorphic structures even record ages of 2.30–2.10 Ga. It is still debatable whether or not the late Neoproterozoic tectonothermal event lasted over such a long period from 2.50 Ga to 2.45 Ga and even later, or whether there were multiple events, or whether the ages of 2.30–2.10 Ga have no geological meaning because of strong late Palaeoproterozoic overprinting (Wan *et al.* 2020).

3. Sampling and petrography

Twelve samples, including TTG gneisses, crustally derived granite gneisses, meta-mafic and intermediate rocks, were collected from the Daqingshan area for detailed investigation. Sample locations are shown in Figure 1. The mineral contents of the dated rock samples are listed in Table 1.

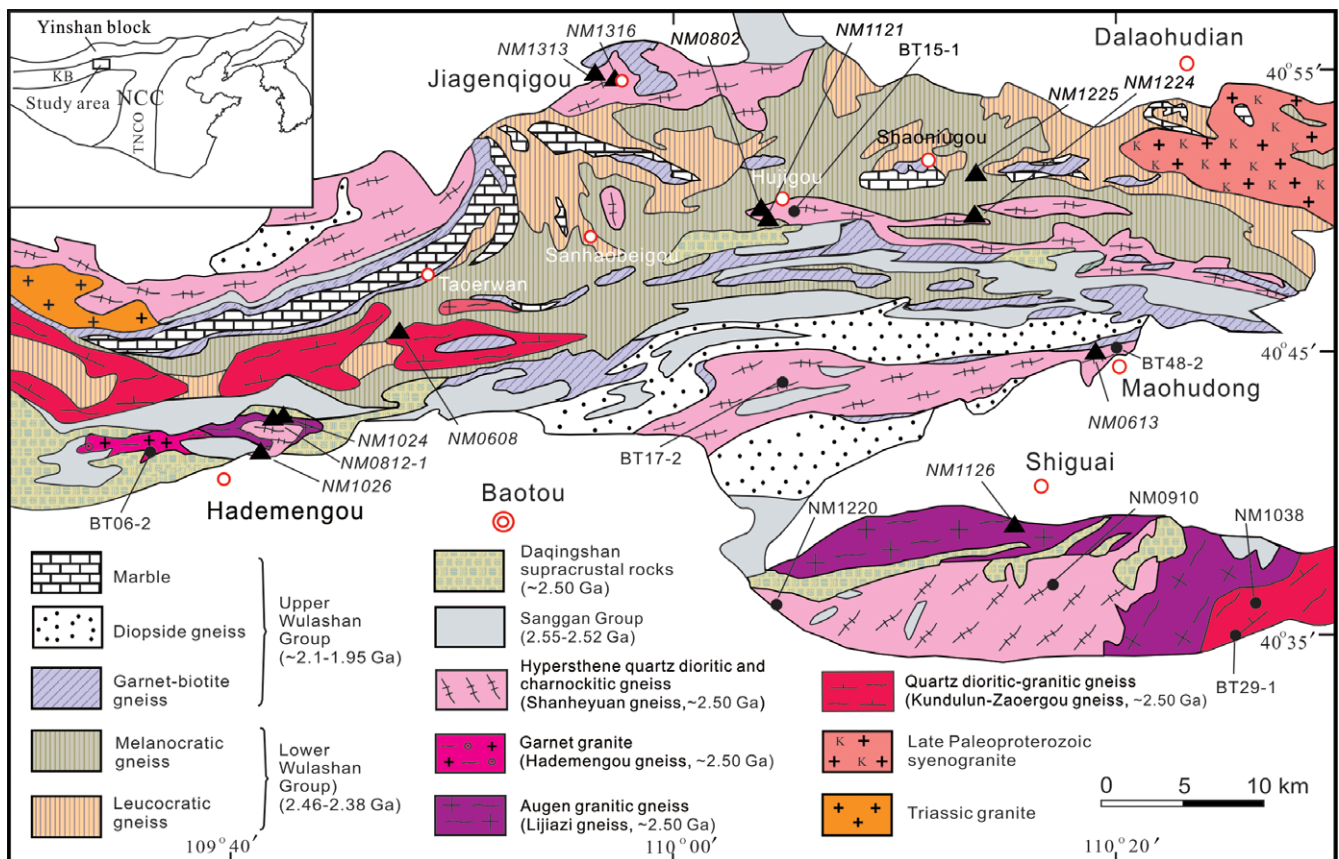


Fig. 1. (Colour online) Geological map of the Daqingshan area, northwestern North China Craton. Modified after Xu *et al.* (2005), with the inset from Zhao *et al.* (2005). Triangles and circles show the locations of samples in this study and in previous studies, respectively.

3.a. TTG gneisses

3.a.1. Trondhjemitic gneiss (NM1224, 40° 49' 54" N, 110° 13' 40" E)

This sample was taken from ~5 km southeast of Shaoniugou. The trondhjemitic gneiss extends in an E–W direction, parallel to its gneissosity (Fig. 2a). It is mainly composed of plagioclase and quartz, with minor biotite and microcline (Fig. 3a). Both plagioclase and quartz show recrystallized boundaries. Aligned biotite flakes, partly altered to chlorite, define a weak foliation.

3.a.2. Trondhjemitic gneiss (NM1225, 40° 51' 15" N, 110° 13' 31" E)

At ~2.5 km north of sample NM1224, a small trondhjemitic body (<1 km²) was identified within the Lower Wulashan Group. The body is cut by mafic dykes and both have undergone granulite-facies metamorphism. The TTG rock locally shows a banded structure, but sample NM1225 was taken from a relatively homogeneous portion (Fig. 2b). It is mainly composed of plagioclase, quartz and mafic minerals, with minor microcline (Fig. 3b). The mafic minerals include hornblende, brown biotite and diopside. Although hypersthene is not observed in thin-section, it has been identified in the outcrop.

3.a.3. Granodiorite augen gneiss (NM0812-1, 40° 42' 53" N, 109° 42' 15" E)

There is a small augen gneiss body (1 × 5 km²) located to the east of the well-known Hademengou garnet granite north of

Hademengou (Fig. 1). This granodiorite augen gneiss separates the Daqingshan Supracrustal Rocks in the north from charnockitic gneiss in the south, and locally contains mafic granulite enclaves (Fig. 2c). The augen gneiss commonly shows strong deformation, but sample NM0812-1 was taken from a relatively weakly deformed outcrop with the largest porphyroblasts up to 8 cm in length (Fig. 2d). It is mainly composed of plagioclase, microcline, quartz, hornblende and biotite (Fig. 3c). The matrix is fine to medium grained with a crystalloblastic structure, and the microcline porphyroblasts commonly contain quartz and plagioclase inclusions. Hornblende and biotite occur together and help to define the foliation.

3.a.4. Granodiorite augen gneiss (NM1126, 40° 38' 57" N, 110° 17' 44" E)

A large granodiorite augen gneiss body extends in an E–W direction to the south of Shiguai (Fig. 1). It encloses and cuts the Daqingshan Supracrustal Rocks (Fig. 2e). The granodiorite body shows large variations in the size and content of microcline porphyroblasts ranging from 2 cm to 10 cm and 30% to 5%, respectively. Commonly, the porphyroblasts decrease in size with their decrease in content. Sample NM1126 was taken from a domain representing the protolith in an outcrop where the granodiorite gneiss locally shows anatexis (Fig. 2f). It is mainly composed of microcline, plagioclase, quartz, biotite and hornblende (Fig. 3d). Oriented biotite and hornblende aggregates and quartz and microcline aggregates define a strong foliation.

Table 1. Summary of mineral contents for the late Neoproterozoic – early Palaeoproterozoic meta-intrusive rocks in the Daqingshan area, northwestern North China Craton

No.	Sample no.	Rock type	Plagioclase (%)	Microcline (%)	Feldspar (%)	Quartz (%)	Biotite (%)	Mafic minerals (%)	Hornblende (%)	Dark minerals (%)	Pyroxene (%)
1	NM1224	Trondhjemitic gneiss	45–50	2–4		45–50	2–4				
2	NM1225	Trondhjemitic gneiss	40–45	3–5		40–45		5–10			
3	NM0812-1	Granodiorite augen gneiss	30–35	20–25		35–40	2–5		3–5		
4	NM1126	Granodiorite augen gneiss	30–35	20–25		35–40	3–5		5–8		
5	NM1313	Quartz monzonite gneiss			48–58	42–47	3–5				
6	NM1316	Mylonitized augen monzogranite	25–30	25–30		40–45					
7	NM0613	Monzogranitic gneiss	25–30	25–30		45–58					
8	NM0802	Meta-diorite	55–60	3–5		3–5				25–30	
9	NM1121	Meta-diorite	55–60	3–5		3–5				25–30	
10	NM0608	Meta-gabbroic diorite	45–50			3–8	2–4		38–43		
11	NM1024	Meta-gabbroic diorite	45–50			2–3			45–50		
12	NM1026	Meta-gabbro	40–45						25–30		25–30

3.b. Quartz monzonite and monzogranite gneisses

3.b.1. Quartz monzonite gneiss (NM1313, 40° 54' 58.53" N, 109° 55' 44.02" E)

At ~1 km west of Jiagenqigou, where the Shanheyuan gneiss crops out (Fig. 1), locally exposed rocks show strong mylonitization with lineations extending in an E–W direction. Sample NM1313 was taken from a relatively fresh outcrop (Fig. 2g). It is mainly composed of feldspar and quartz, with minor biotite (Fig. 3e, f). The high K₂O content (4.82%) of the rock suggests that some untwinned feldspar may also be K-feldspar. Recrystallized quartz bands and oriented biotite flakes define a strong foliation.

3.b.2. Mylonitized augen monzogranite (NM1316, 40° 54' 17.53" N, 109° 57' 10.45" E)

This sample was taken from ~200 m west of Jiagenqigou, where augen gneisses are well developed. They commonly show strong mylonitization (Fig. 2h), and the mylonite foliation and mafic dykes are folded (Fig. 2i). Sample NM1316 is mainly composed of microcline, plagioclase and quartz, with minor biotite. Microcline occurs as phenocrysts/augen (not shown here). Recrystallized quartz bands define a strong foliation (Fig. 3g). There are fine-grained mineral aggregates of plagioclase, microcline and quartz.

3.b.3. Monzogranitic gneiss (NM0613, 40° 45' 04" N, 110° 19' 01" E)

This sample was collected from ~2 km northwest of Maohudong. The rock is homogeneous in mineral contents and is grey on fresh surfaces, but pinkish on weathered surfaces (Fig. 2j), being different from what is named on the geological map as hypersthene-

quartz dioritic and charnockitic gneisses. Granulites occur as enclaves in the monzogranitic gneiss. Sample NM0613 is mainly composed of plagioclase, microcline and quartz (Fig. 3h, i), being similar in petrographic features to sample NM1313, but containing less microcline phenocrysts.

3.c. Meta-gabbros and diorites

3.c.1. Meta-diorite (NM0802, 40° 50' 00" N, 110° 03' 47" E)

This sample was taken from the Shanheyuan gneiss, ~1 km southwest of Hujigou (Fig. 1). In a N–S section along the road, granitoid rocks commonly show a banded structure, partly because of anatexis. Sample NM0802 was taken from an outcrop with relatively homogeneous mineral contents (Fig. 2k). It is mainly composed of plagioclase and dark minerals, with some quartz and microcline (Fig. 3j, k). Plagioclase shows a crystalloblastic structure. Dark minerals include biotite and hornblende that occur as aggregates defining a weak foliation.

3.c.2. Meta-diorite (NM1121, 40° 49' 47" N, 110° 04' 02" E)

This sample was also collected from the Shanheyuan gneiss, ~1 km south of sample NM0802 (Fig. 1). It is similar in field and petrographic features to sample NM0802, but shows strong deformation (Figs 2l, 3l, m).

3.c.3. Meta-gabbroic diorite (NM0608, 40° 46' 12" N, 109° 47' 37" E)

This sample was taken from the Kundulun–Zaogou gneiss, ~3 km southwest of Taoerwan (Fig. 1). The meta-gabbroic diorite occurs on a relatively large scale. The rock is homogeneous in



Fig. 2. (Colour online) Field photographs of the late Neoproterozoic – early Palaeoproterozoic meta-plutonic rocks in the Daqingshan area, northwestern North China Craton. (a) Trondhjemitic gneiss (NM1224), ~5 km northeast of Shaoniugou. (b) Trondhjemitic gneiss (NM1225), ~2.5 km northeast of Shaoniugou. (c, d) Granodiorite augen gneiss (NM0812-1), containing granulite enclaves, ~3 km northeast of Hademengou. (e) Granodiorite augen gneiss cutting the Daqingshan Supracrustal Rocks. (f) The site of sample NM1126, ~2 km south of Shiguai. (g) Quartz monzonite gneiss (NM1313), showing strong deformation, ~500 m west of Jiagenqigou. (h, i) Mylonitized augen monzogranite (NM1316), intruded by mafic dykes, ~200 m west of Jiagenqigou. (j) Monzogranitic gneiss (NM0613), ~2 km northwest of Maohudong. (k) Meta-diorite (NM0802), ~1 km west of Hujigou. (l) Meta-diorite (NM1121), ~3 km east of Hujigou. (m) Meta-gabbroic diorite (NM0608), ~3 km southwest of Taoerwan. (n) Meta-gabbroic diorite (NM1024), ~6 km northeast of Hademengou. (o, p) Meta-gabbro (NM1026), with granulite enclaves, ~2 km northeast of Hademengou. The marker pen for scale is 14 cm in length.



Fig. 2. (Continued)

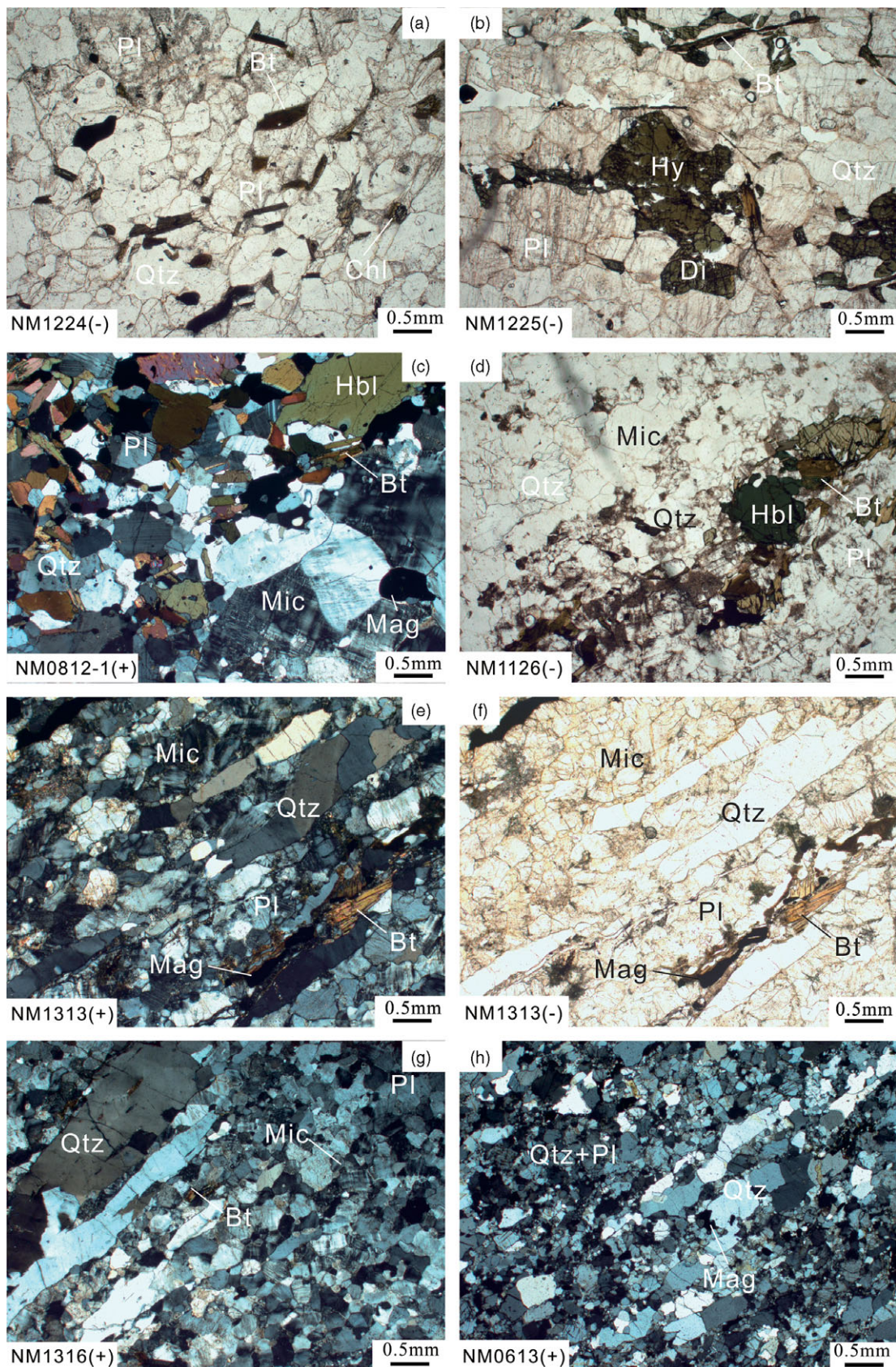


Fig. 3. (Colour online) Photomicrographs showing petrographic features of the late Neoproterozoic – early Palaeoproterozoic meta-plutonic rocks in the Daqingshan area, northwestern North China Craton. (a) Trondhjemitic gneiss (NM1224). (b) Trondhjemitic gneiss (NM1225). (c) Granodiorite augen gneiss (NM0812-1). (d) Granodiorite augen gneiss (NM1126). (e, f) Quartz monzonite gneiss (NM1313). (g) Mylonitized augen monzogranite (NM1316). (h, i) Monzogranitic gneiss (NM0613). (j, k) Meta-diorite (NM0802). (l, m) Meta-diorite (NM1121). (n) Meta-gabbroic diorite (NM0608). (o) Meta-gabbroic diorite (NM1024). (p) Meta-gabbro (NM1026). (+) and (–) represent cross- and plane-polarized light, respectively. Mineral symbols: Bt – biotite; Pl – plagioclase; Qtz – quartz; Chl – chlorite; Hbl – hornblende; Mic – microcline; Di – diopside; Px – pyroxene; Mag – magnetite; Ep – epidote; Cpx – clinopyroxene.

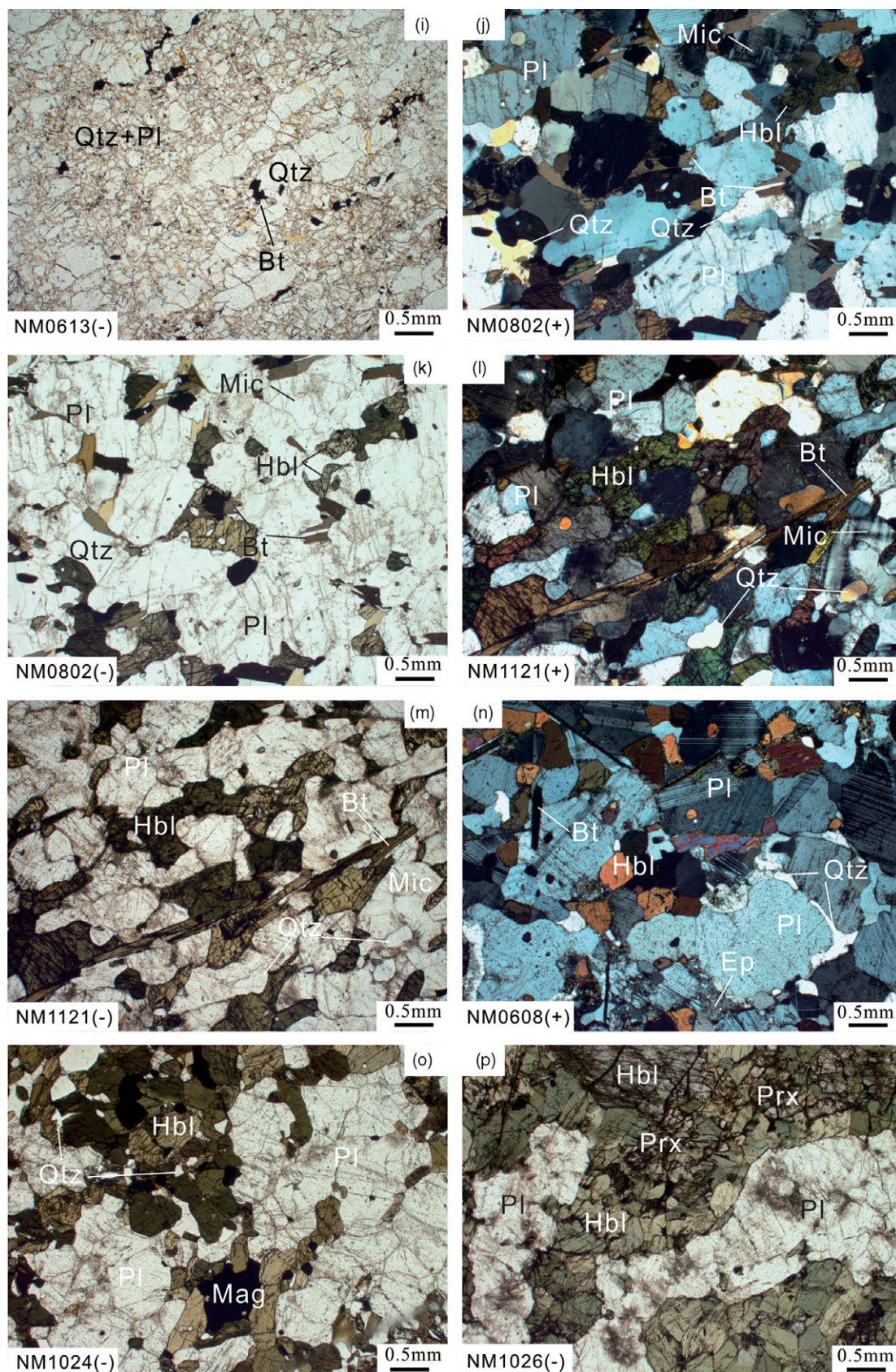


Fig. 3. (Continued)

mineral contents, and shows weak anatexis in outcrop, with some small red granitic dykes (Fig. 2m). It is mainly composed of plagioclase and hornblende, with lesser amounts of biotite and quartz (Fig. 3n). Some plagioclase shows polysynthetic twinning. Biotite commonly occurs together with hornblende. There are local, fine-grained felsic mineral aggregates between coarse-grained plagioclase grains, which are considered to be a result of anatexis.

3.c.4. Meta-gabbroic diorite (NM1024, 40° 43' 01" N, 109° 42' 30" E)

To the north of sample NM0812-1, ~6 km northeast of Hademengou (Fig. 1), granodiorite augen gneiss was intruded by a gabbroic diorite dyke. The dyke is ~40 m in width and extends in an E–W direction. The dyke is homogeneous with only a few leucosomes of probable anatectic origin (Fig. 2n). It is mainly composed of plagioclase and hornblende, with minor quartz (Fig. 3o). Plagioclase shows recrystallized boundaries with some altered to epidote. Some fine-grained quartz occurs in hornblende aggregates.

3.c.5. Meta-gabbro (NM1026, 40° 41' 54" N, 109° 40' 58" E)

This sample was taken from ~2 km northeast of Hademengou (Fig. 1). It is a small meta-gabbro body in which there are mafic granulite and meta-pyroxenite enclaves showing a transitional relationship (Fig. 2o, p). The meta-gabbro is cut by granite dykes (Fig. 2o) and is mainly composed of pyroxene, hornblende and plagioclase (Fig. 3p). Some plagioclase is altered to epidote.

4. Analytical techniques

Zircon separation, cathodoluminescence (CL) imaging and zircon dating were carried out at the Beijing SHRIMP Centre, Chinese Academy of Geological Sciences (CAGS), Beijing. Age measurements were performed over a long period, but in all cases the analytical procedures and conditions were similar to those described by Williams (1998). Mass resolution during the analytical sessions was ~5000 (1 % height). The intensity of the primary O_2^- ion beam was 3–5 nA, and spot sizes were 25–30 μm , with each analytical site rastered for 2–3 minutes prior to analysis. Five scans through the mass stations were made for each age determination. Reference standard zircons used were M257 ($U = 840$ ppm, Nasdala *et al.* 2008) and TEMORA 1 (^{206}Pb – ^{238}U age = 417 Ma, Black *et al.* 2003). A common lead correction was applied using the measured ^{204}Pb abundances and Cumming & Richards (1975) common Pb composition for the likely age of the rocks. Data processing and assessment was carried out using the SQUID and Isoplot programs (Ludwig, 2001, 2003). Uncertainties in the isotopic ratios of individual analyses and on the concordia diagrams are given at 1σ , whereas uncertainties for weighted mean ages in the text are quoted at the 95 % confidence level.

In situ zircon Hf isotopic analyses for samples NM0608, NM0613, NM1024, NM1313 and NM1316 were conducted with a Nu Plasma II multi-collector (MC)-ICP-MS connected to a RESOLUTION M-50 193 nm laser system at the State Key Laboratory of Continental Dynamics, Northwest University, Xi'an. Details of the analytical procedure were described by Yuan *et al.* (2008). In all cases, *in situ* Lu–Hf analyses of zircons were conducted on the pits generated during U–Pb dating or a nearby area with the same internal structures as determined by CL. The spot size was 44 μm , while the laser repetition rate was 6 Hz and the energy density was 6 J cm^{-2} . The obtained $^{176}\text{Hf}/^{177}\text{Hf}$ ratios of the GJ-1 and Mud Tank standards were

0.282008 ± 0.000028 ($n = 20$, 2σ) and 0.282500 ± 0.000021 ($n = 20$, 2σ ; see online Supplementary Material Table S1 for details), respectively, which almost reproduced the recommended $^{176}\text{Hf}/^{177}\text{Hf}$ ratios (0.282015 ± 0.000019 , 2σ ; 0.282507 ± 0.000006 , 2σ) (Woodhead & Hergt, 2005; Elhlou *et al.* 2006). For the remaining samples, analyses were carried out using a Geolas-193 laser-ablation microprobe, attached to a Neptune MC-ICP-MS, at the Institute of Mineral Resources (IMR), CAGS, and the Tianjin Institute of Geology and Mineral Resources (TIGMR), China Geological Survey, Tianjin. The detailed analytical procedures were described by Hou *et al.* (2007). Analyses were carried out using a spot size of 55 μm . Ablation times were ~26 s for 200 cycles constituting each measurement, with an 8 Hz repetition rate, and a laser power of 100 mJ/pulse. The $^{176}\text{Hf}/^{177}\text{Hf}$ ratios of the GJ-1 standard during Hf isotopic analysis at IMR and TIGMR were 0.282011 ± 0.000018 (2σ , $n = 50$) and 0.282009 ± 0.000016 (2σ , $n = 28$; see online Supplementary Material Table S2 for details), respectively. They reproduced the recommended $^{176}\text{Hf}/^{177}\text{Hf}$ ratio (GJ-1: 0.282015 ± 0.000019 (2σ); Elhlou *et al.* 2006). The decay constant for ^{176}Lu of 1.867×10^{-11} year $^{-1}$ (Söderlund *et al.* 2004), and the present-day chondritic ratios of $^{176}\text{Hf}/^{177}\text{Hf} = 0.28325$ and $^{176}\text{Lu}/^{177}\text{Hf} = 0.0336$ (Bouvier *et al.* 2008) were adopted to calculate $\epsilon_{\text{Hf}}(t)$ values. Single-stage Hf model ages (t_{DM1}) were calculated by reference to depleted mantle with a present-day $^{176}\text{Hf}/^{177}\text{Hf}$ ratio of 0.28325 and $^{176}\text{Lu}/^{177}\text{Hf}$ ratio of 0.0384, and two-stage Hf model ages (t_{DM2}) were calculated by assuming a mean $^{176}\text{Lu}/^{177}\text{Hf}$ value of 0.015 (Griffin *et al.* 2002) for the average continental crust.

This study presents elemental and Sm–Nd isotopic analyses on 15 and 11 samples, respectively. All samples were powdered to 200-mesh in an agate mill. Whole-rock element analyses were conducted at the National Research Centre of Geoanalysis, CAGS, Beijing. Major elements were determined by X-ray fluorescence spectrometry (XRF), with FeO and Fe $_2$ O $_3$ contents determined by the wet chemical method. The analytical precision (1σ) for all major-element oxides is better than 2 %. Trace elements were separated using cation-exchange techniques and analysed by ICP-MS. Uncertainties are ~10 % and ~5 % for elements with abundances of ~10 ppm and ~10 ppm, respectively. The recommended and measured values of standards GBW07103, GBW07107, GBW07122 and GBW07123 are listed in online Supplementary Material Table S3, which are close to each other. Whole-rock Sm–Nd isotopic analyses were carried out in the Laboratory of Isotope Geology, CAGS, with the procedures similar to those described by Zhang & Ye (1987). The $^{143}\text{Nd}/^{144}\text{Nd}$ ratio of the JMC-Nd standard during Sm–Nd isotopic analysis in the Laboratory of Isotope Geology, CAGS, was 0.511126 ± 5 (SD), which is close to the recommended $^{143}\text{Nd}/^{144}\text{Nd}$ ratio (JMC-Nd: 0.511134 ± 38 (SD); Zhang *et al.* & Hu, 2020). The Nd model ages reported here are based on the depleted mantle model of DePaolo (1988).

5. Zircon geochronology

Using the CL imaging, Th/U ratios and ages, the analysed zircons were identified as magmatic (MA), recrystallized (RC), overgrowth (rim, R) or xenocrystic (X). Magmatic zircon commonly shows oscillatory zoning; recrystallized zircon refers to that in which the original texture has been modified under thermal and fluid conditions, such as the disappearance or blurring of magmatic zoning. Overgrowth zircon refers to zircon newly grown during metamorphism. Xenocrystic zircon is older than magmatic zircon but

can keep magmatic zoning. In some or even many cases, it is difficult to determine the origin (recrystallization or overgrowth) of the metamorphic rims. U–Pb data are listed in online Supplementary Material Table S4.

5.a. TTG gneisses

5.a.1. Trondhjemitic gneiss (NM1224)

The zircons are subhedral and tabular in shape and some show core–rim structures in CL images (Fig. 4a). Magmatic cores mostly show oscillatory zoning, whereas recrystallized or overgrowth rims are homogeneous. Twenty-six analyses were performed on 24 zircon grains. Nine analyses on magmatic domains have U contents and Th/U ratios of 30–166 ppm and 0.25–1.17, respectively. Seven of them are concordant to slightly discordant (discordance $\leq 2\%$), with a weighted mean ^{207}Pb – ^{206}Pb age of 2516 ± 9 Ma (MSWD = 0.25; Fig. 5a). Four analyses (10.1R, 11.1R, 12.1R, 17.1R) on rims have U contents of 132–179 ppm, Th/U ratios of 0.3–0.7 and record a weighted mean ^{207}Pb – ^{206}Pb age of 1870 ± 11 Ma (MSWD = 2.0). Other analyses on recrystallized and overgrowth domains have U contents of 100–855 ppm, Th/U ratios of 0.01–0.35 and ^{207}Pb – ^{206}Pb ages ranging from 2460 to 2012 Ma. Five analyses (8.1R+RC, 13.1R, 19.1R, 20.1R, 21.1R) with low Th/U ratios of 0.01–0.07 have ^{207}Pb – ^{206}Pb ages of 2442–2418 Ma.

5.a.2. Trondhjemitic gneiss (NM1225)

The zircons are stubby or oval in shape and have oscillatory zoning, with some having narrow rims in CL images (Fig. 4b). Twenty-seven analyses were performed on 22 zircons. Seventeen analyses on magmatic domains have U contents and Th/U ratios of 151–541 ppm and 0.47–1.30, respectively. Seventeen of them are on or close to concordia and have ^{207}Pb – ^{206}Pb ages ranging from 2488 Ma to 2410 Ma (Fig. 5b). Among them, four analyses (1.1MA, 2.1MA, 20.1MA, 22.1MA) with the oldest ages yield a weighted mean ^{207}Pb – ^{206}Pb age of 2486 ± 7 Ma (MSWD = 0.04). Three analyses (7.1R, 8.1R, 11.1R) on rims have U contents of 893–1028 ppm and Th/U ratios of 0.08–0.15; among them, analyses 8.1R and 11.1R have a weighted mean ^{207}Pb – ^{206}Pb age of 1844 ± 9 Ma (MSWD = 0.03).

5.a.3. Granodiorite augen gneiss (NM0812-1)

The zircons are tabular in shape and have banded or oscillatory zoning, with evidence of internal recrystallization, and they also have narrow recrystallized or overgrowth rims (Fig. 4c). Thirty-one analyses were performed on 26 zircon grains. Eleven analyses on magmatic domains have U contents and Th/U ratios of 189–398 ppm and 0.41–1.53, respectively. All of them are on or close to concordia and have ^{207}Pb – ^{206}Pb ages ranging almost continuously from 2478 Ma to 2395 Ma. Three analyses (2.1MA, 12.1MA, 13.1MA) with the oldest ages yield a weighted mean ^{207}Pb – ^{206}Pb age of 2474 ± 12 Ma (MSWD = 0.18; Fig. 5c). Twenty analyses on recrystallized or overgrowth domains have U contents of 135–410 ppm, Th/U ratios of 0.05–0.79 and ^{207}Pb – ^{206}Pb ages ranging from 2503 Ma to 1856 Ma. It is notable that on grain 18, the recrystallized rim (18.1RC) has an older ^{207}Pb – ^{206}Pb age (2503 ± 15 Ma, discordance = -1%) than the magmatic core (18.2MA, 2455 ± 9 Ma, discordance = 3%). The youngest rim (14.2R) has a Th/U ratio of 0.08 and a ^{207}Pb – ^{206}Pb age of 1856 ± 13 Ma (discordance = -2% ; Figs 4c, 5c).

5.a.4. Granodiorite augen gneiss (NM1126)

The zircons are subhedral and tabular in shape and some show core–rim structures in CL images (Fig. 4d). Magmatic cores have oscillatory zoning, whereas the recrystallized or overgrowth rims are more homogeneous. Commonly, there are light seams around the cores, indicating fluid-present recrystallization (Fig. 4d). Eighteen analyses were performed on 14 zircon grains. Nine analyses on magmatic domains have U contents and Th/U ratios of 77–337 ppm and 0.61–1.08, respectively. The zircons have undergone radiogenic lead loss to different degrees, but all analyses define a discordia (Fig. 5d). Two analyses (6.1MA, 7.1MA) closest to concordia yield a weighted mean ^{207}Pb – ^{206}Pb age of 2510 ± 14 Ma (MSWD = 0.08). Five analyses on recrystallized or overgrowth rims have U contents of 207–640 ppm and Th/U ratios of 0.31–0.47; they also show radiogenic lead loss with a similar distribution to magmatic zircons. Two analyses (6.2RC, 8.1RC) closest to concordia have a weighted mean ^{207}Pb – ^{206}Pb age of 2496 ± 13 Ma (MSWD = 0.08). Four analyses on rim domains have U contents of 184–690 ppm and Th/U ratios of 0.03–0.11. They roughly constitute another discordia, with analysis 5.1R that is closest to concordia having a ^{207}Pb – ^{206}Pb age of 1956 ± 10 Ma.

5.b. Quartz monzonite and monzogranitic gneisses

5.b.1. Quartz monzonite gneiss (NM1313)

The zircons are stubby or oval in shape and have oscillatory zoning, with evidence of internal recrystallization and recrystallized or overgrowth rims (Fig. 4e). Twenty-five analyses were performed on 23 zircon grains, and 20 of them are distributed on or close to concordia (discordance $\leq 3\%$; Fig. 5e). Eight analyses on magmatic domains have U contents and Th/U ratios of 184–347 ppm and 0.41–0.76, respectively, and show large ^{207}Pb – ^{206}Pb age variations from 2396 Ma to 2188 Ma (Fig. 5e). Four analyses on recrystallized domains have higher U contents and lower Th/U ratios than the magmatic domains, but show similar ^{207}Pb – ^{206}Pb age variations. Thirteen analyses on recrystallized or overgrowth rims have U contents of 64–891 ppm and show higher Th/U ratios of 0.02–2.26 and ^{207}Pb – ^{206}Pb age variations of 2402–1887 Ma. Analysis 4.1R on a rim has the highest Th/U ratio of 2.26 and the youngest ^{207}Pb – ^{206}Pb age of 1887 Ma. Similar to zircons from sample NM0812-1, some rims have older ^{207}Pb – ^{206}Pb ages than cores (grains 18 and 22 in Fig. 5e).

5.b.2. Mylonitized augen monzogranite (NM1316)

The zircons are subhedral and tabular in shape and show recrystallization to different degrees, with little magmatic zoning remaining. They also have recrystallized or overgrowth rims; core–rim structures are common (Fig. 4f). Fifteen analyses were performed on 15 zircon grains, and are concentrated in four populations on the concordia diagram (Fig. 5f), with a similar distribution to zircons from sample NM1313. Nine analyses on recrystallized domains have U contents and Th/U ratios of 229–1310 ppm and 0.24–1.10, respectively, and have ^{207}Pb – ^{206}Pb ages of 2414–2008 Ma (Fig. 5f). Six analyses on recrystallized or overgrowth rims have U contents of 249–2124 ppm and Th/U ratios of 0.10–0.56. Analysis 3.1R has a Th/U ratio of 0.10 and a ^{207}Pb – ^{206}Pb age of 2304 Ma (discordance = 13%). The remaining analyses are concentrated in two locations on concordia, with weighted mean ^{207}Pb – ^{206}Pb ages of 1951 ± 7 Ma (MSWD = 0.22) and 1884 ± 19 Ma (MSWD = 0.003).

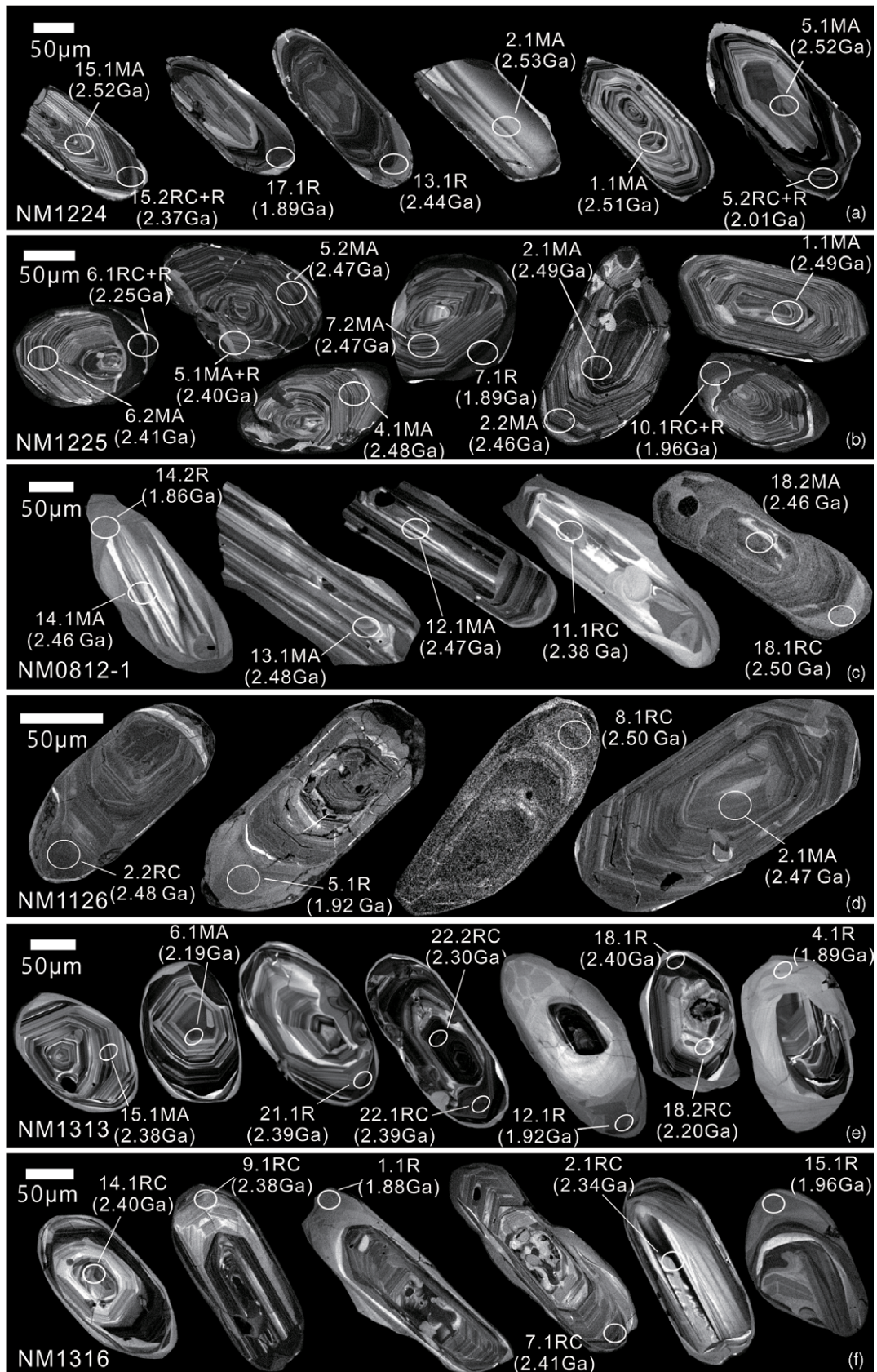


Fig. 4. Cathodoluminescence images of zircons from the late Neoproterozoic – early Palaeoproterozoic meta-plutonic rocks in the Daqingshan area, northwestern North China Craton. (a) Trondhjemitic gneiss (NM1224). (b) Trondhjemitic gneiss (NM1225). (c) Granodiorite augen gneiss (NM0812-1). (d) Granodiorite augen gneiss (NM1126). (e) Quartz monzonite gneiss (NM1313). (f) Mylonitized augen monzogranite (NM1316). (g) Monzogranitic gneiss (NM0613). (h) Meta-diorite (NM0802). (i) Meta-diorite (NM1121). (j) Meta-gabbroic diorite (NM0608). (k) Meta-gabbroic diorite (NM1024). (l) Meta-gabbro (NM1026). MA – magmatic; RC – recrystallized; X – xenocrystic; R – overgrowth (rim).

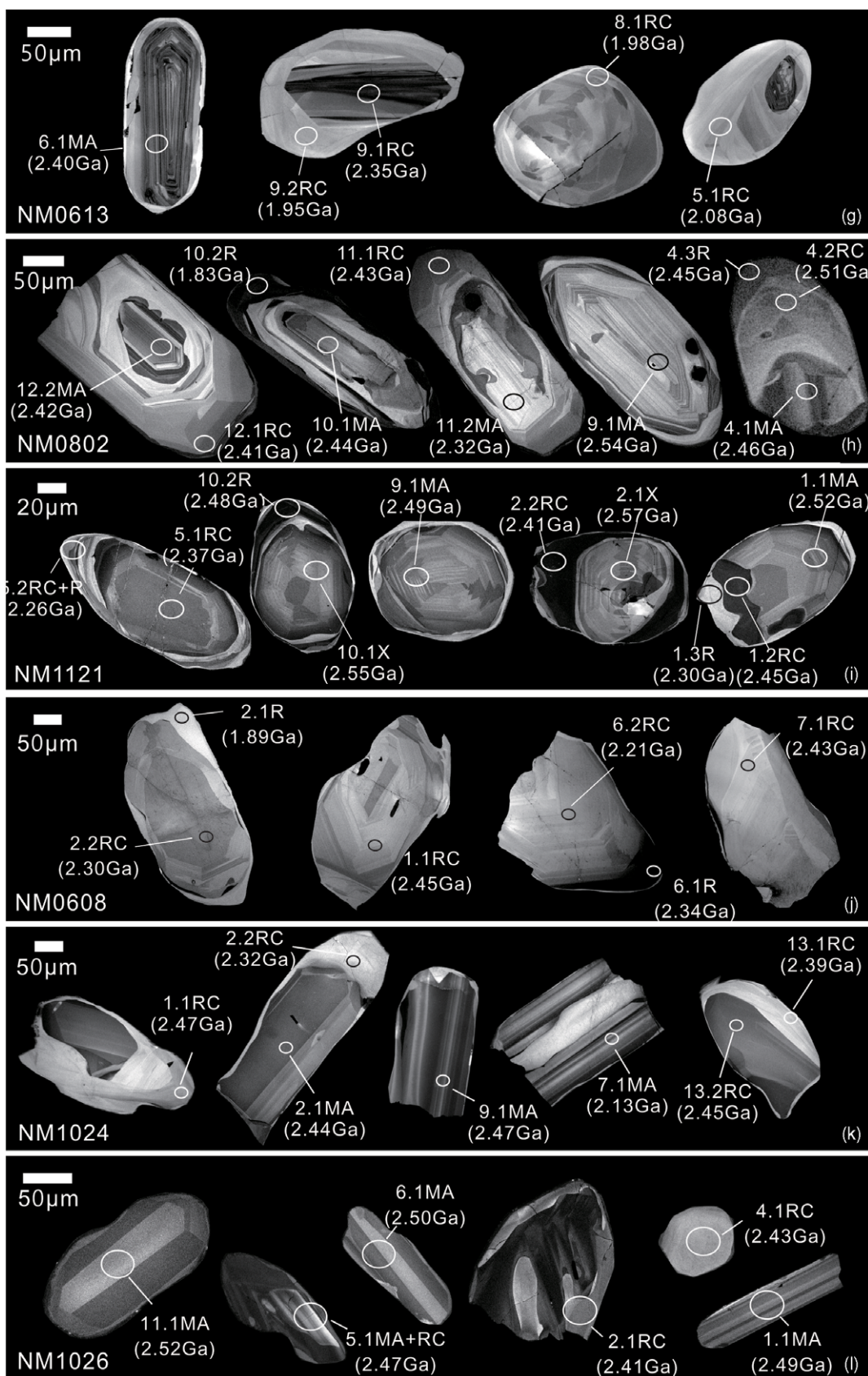


Fig. 4. (Continued)

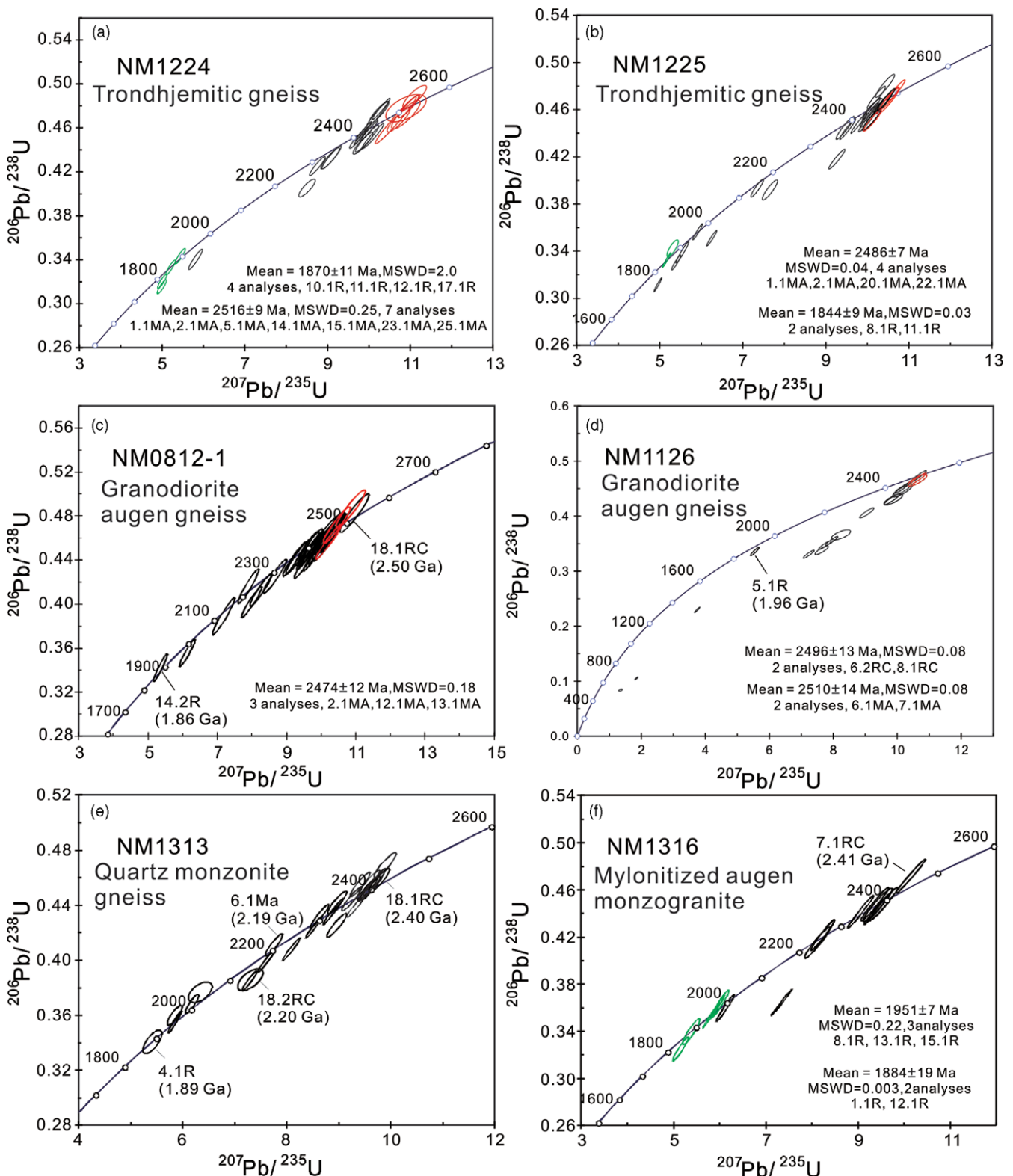


Fig. 5. (Colour online) Concordia diagrams showing SHRIMP U-Pb zircon analyses of the late Neoproterozoic – early Palaeoproterozoic meta-plutonic rocks in the Daqingshan area, northwestern North China Craton. (a) Trondhjemitic gneiss (NM1224). (b) Trondhjemitic gneiss (NM1225). (c) Granodiorite augen gneiss (NM0812-1). (d) Granodiorite augen gneiss (NM1126). (e) Quartz monzonite gneiss (NM1313). (f) Mylonitized augen monzogranite (NM1316). (g) Monzogranitic gneiss (NM0613). (h) Meta-diorite (NM0802). (i) Meta-diorite (NM1121). (j) Meta-gabbroic diorite (NM0608). (k) Meta-gabbroic diorite (NM1024). (l) Meta-gabbro (NM1026). Red ellipses represent the magmatic and green ellipses the metamorphic zircon data used for age calculations.

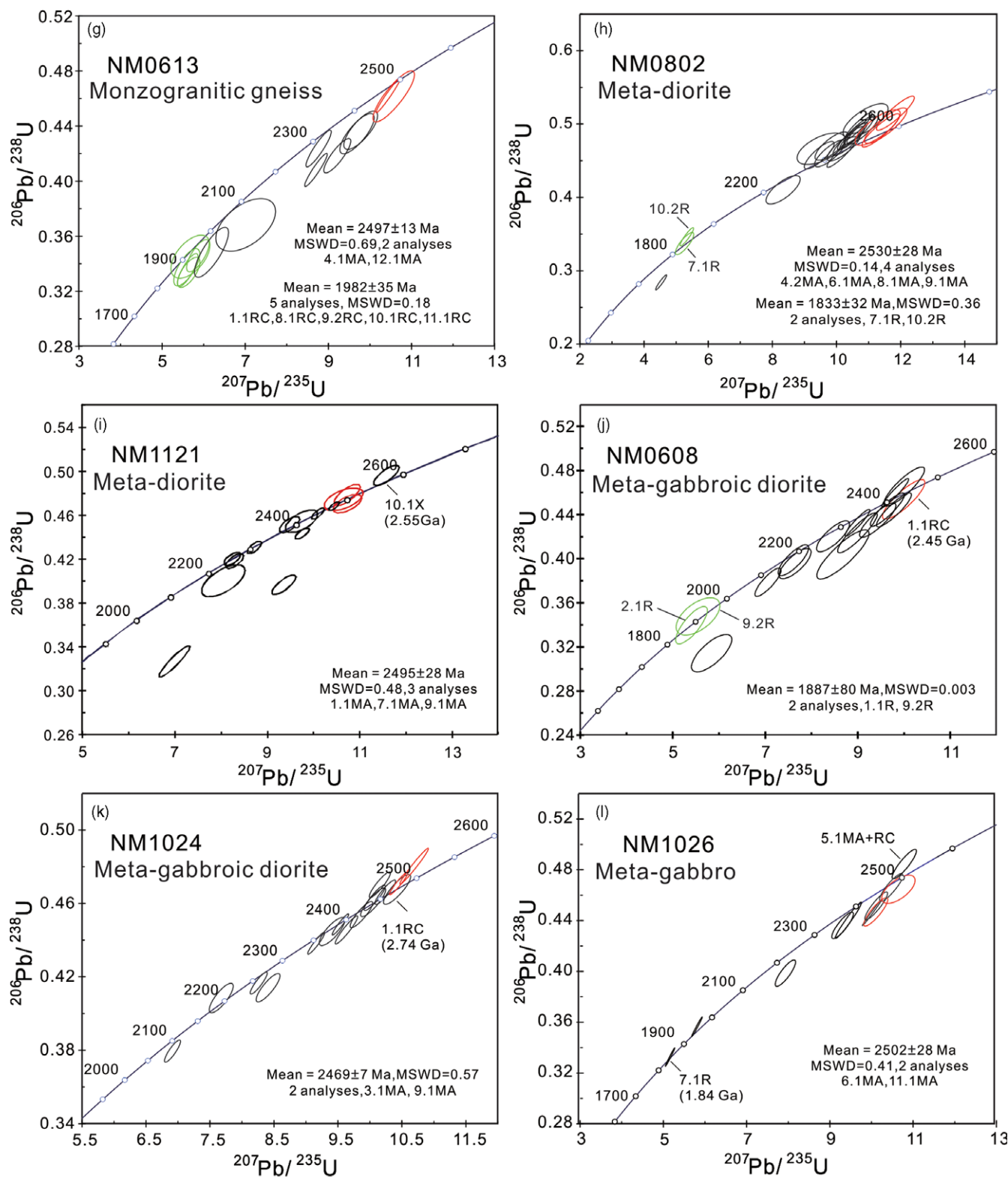


Fig. 5. (Continued)

5.b.3. Monzogranitic gneiss (NM0613)

The zircons are oval, stubby or tabular in shape and show oscillatory and banded zoning, with evidence of strong recrystallization that commonly forms core-rim structures (Fig. 4g). Fourteen

analyses were performed on 13 zircon grains. Six analyses on magmatic domains have U contents of 53–459 ppm and Th/U ratios of 0.52–1.64. They show radiogenic lead loss to different degrees but are roughly distributed along a discordia (Fig. 5g). Two analyses

closest to concordia yield a weighted mean ^{207}Pb – ^{206}Pb age of 2497 ± 13 Ma (MSWD = 0.69). Eight analyses on recrystallized domains have U contents of 27–271 ppm and Th/U ratios 0.13–0.97. Five of them are concentrated on concordia and yield a weighted mean ^{207}Pb – ^{206}Pb age of 1982 ± 35 Ma (MSWD = 0.18).

5.c. Meta-gabbros and diorites

5.c.1. Meta-diorite (NM0802)

The zircons are stubby to tabular in shape and show oscillatory zoning with some displaying recrystallization and overgrowth rims in CL images, defining core–rim structures (Fig. 4h). Twenty-one analyses were carried out on 12 zircon grains. Ten analyses on magmatic domains have U contents and Th/U ratios of 24–98 ppm and 0.62–3.94, respectively, and are concentrated along concordia, with ^{207}Pb – ^{206}Pb ages of 2538–2323 Ma; four of them with the oldest ages define a weighted mean ^{207}Pb – ^{206}Pb age of 2530 ± 28 Ma (MSWD = 0.14) (Fig. 5h). Six analyses on recrystallization domains have U contents of 36–96 ppm, Th/U ratios 0.79–1.49 and ^{207}Pb – ^{206}Pb ages of 2510–2315 Ma. Four analyses on recrystallized or overgrowth rims have U contents of 47–387 ppm and Th/U ratios 0.05–1.44. Analysis 4.3R has the oldest ^{207}Pb – ^{206}Pb age of 2450 ± 25 Ma, whereas analyses 7.1R and 10.2R yield a weighted mean ^{207}Pb – ^{206}Pb age of 1833 ± 32 Ma (MSWD = 0.36).

5.c.2. Meta-diorite (NM1121)

The zircons are oval to stubby in shape and show core–rim structures in CL images (Fig. 4i). Magmatic cores are homogeneous or have oscillatory zoning, with evidence of recrystallization, together with thin recrystallized or overgrowth rims. Fifteen analyses were performed on ten zircon grains. Three analyses on magmatic domains have U contents and Th/U ratios of 68–119 ppm and 0.79–0.85, respectively, and yield a weighted mean ^{207}Pb – ^{206}Pb age of 2495 ± 28 Ma (MSWD = 0.48) (Fig. 5i). Six analyses on recrystallized domains have U contents of 141–1102 ppm, Th/U ratios of 0.16–1.13 and ^{207}Pb – ^{206}Pb ages of 2453–2275 Ma. Three analyses on recrystallized or overgrowth rims have U contents of 60–725 ppm and Th/U ratios 0.07–0.47, with the oldest ^{207}Pb – ^{206}Pb age being 2475 ± 8 Ma (10.2R). Analysis 10.1X lies on concordia and has a ^{207}Pb – ^{206}Pb age of 2551 ± 17 Ma, which is older than the magmatic zircon, and is probably xenocrystic in origin.

5.c.3. Meta-gabbroic diorite (NM0608)

The zircons are anhedral, stubby to weakly elongated in shape and almost all show recrystallization, with some having recrystallized or overgrowth rims in CL images (Fig. 4j). Sixteen analyses were carried out on 12 zircon grains. Ten analyses on recrystallized domains have U contents and Th/U ratios of 31–61 ppm and 0.64–1.38, respectively, and show large ^{207}Pb – ^{206}Pb age variations from 2452 Ma to 2167 Ma along concordia (Fig. 5j). Six analyses on recrystallized or overgrowth rims have U contents and Th/U ratios of 18–249 ppm and 0.57–0.68, respectively. As with the recrystallized zircons, they also show large, but younger, ^{207}Pb – ^{206}Pb age variations from 2411 Ma to 1886 Ma. Analyses 2.1R and 9.2R record the youngest ages and yield a weighted mean ^{207}Pb – ^{206}Pb age of 1887 ± 80 Ma (MSWD = 0.003), with a large error.

5.c.4. Meta-gabbroic diorite (NM1024)

The zircons are elongate to irregular in shape, and are either homogeneous or show banded zoning with some evidence of

recrystallization in CL images (Fig. 4k). Sixteen analyses were performed on 14 zircon grains, and they are distributed on or close to concordia (Fig. 5k). Eight analyses on magmatic domains have U contents of 111–526 ppm, Th/U ratios of 0.38–1.00 and large ^{207}Pb – ^{206}Pb age variations from 2471 Ma to 2127 Ma. Two analyses (3.1MA, 9.1MA) with the oldest ^{207}Pb – ^{206}Pb ages yield a weighted mean ^{207}Pb – ^{206}Pb age of 2469 ± 7 Ma (MSWD = 0.57). Eight analyses on recrystallization domains have U contents of 64–217 ppm and Th/U ratios of 0.23–0.45. They have similar ^{207}Pb – ^{206}Pb age variations to the magmatic zircon, ranging from 2474 Ma to 2181 Ma.

5.c.5. Meta-gabbro (NM1026)

The zircons show similar features to those from sample NM1024, although banded zoning is less pronounced (Fig. 4l). Eleven analyses were performed on 11 zircons. Five analyses on magmatic domains have U contents and Th/U ratios of 177–1766 ppm and 0.58–0.87, respectively. They are distributed on a discordia line, and two of them (6.1MA, 11.1MA) with the oldest ^{207}Pb – ^{206}Pb ages yield a weighted mean ^{207}Pb – ^{206}Pb age of 2502 ± 28 Ma (MSWD = 0.41; Fig. 5l). Six analyses on recrystallized or overgrowth rims have U contents and Th/U ratios of 112–2161 ppm and 0.09–0.60, respectively. They show large ^{207}Pb – ^{206}Pb age variations from 2408 Ma to 1841 Ma, but with the latter (7.1R) being concordant.

6. Zircon Lu–Hf isotopes

In situ Lu–Hf isotopic analysis was carried out on zircons from all dated samples, including those dated by Xu *et al.* (2015) (online Supplementary Material Table S5). Magmatic zircons from four TTG samples are similar to each other in Hf isotopic compositions. They show large variations in $\epsilon_{\text{Hf}}(t)$ values from -1.1 to $+6.2$ (Fig. 6), corresponding to $t_{\text{DM1}}(\text{Hf})$ and $t_{\text{DM2}}(\text{Hf})$ model ages of 2.7–2.5 Ga and 2.8–2.6 Ga, respectively (Fig. 7). Magmatic zircons from the quartz monzonite and monzogranite gneisses (four samples) have $\epsilon_{\text{Hf}}(t)$ values of -0.95 to $+7.5$, $t_{\text{DM1}}(\text{Hf})$ of 2.9–2.5 Ga and $t_{\text{DM2}}(\text{Hf})$ of 3.1–2.5 Ga, being similar in Hf isotopic composition to those of magmatic zircons from the TTG gneisses. Magmatic zircons from seven gabbroic and dioritic rocks have similar Hf isotopic compositions to those from granitoid rocks, with $\epsilon_{\text{Hf}}(t)$ and $t_{\text{DM1}}(\text{Hf})$ values being -3.4 to $+7.3$ and 2.8–2.5 Ga, respectively. Recrystallized and overgrowth zircon domains are similar in Hf isotopic composition to the magmatic domains, except for some from monzogranitic gneiss sample NM0613, which have more negative $\epsilon_{\text{Hf}}(t)$ values (Fig. 6).

7. Whole-rock elemental and isotopic compositions

7.a. Whole-rock geochemistry

Whole-rock oxide and element compositions for all samples dated in this study, together with those for three samples dated by Xu *et al.* (2015), are listed in online Supplementary Material Table S6. Four TTG gneiss samples have SiO_2 of 61.48–69.77%, TFeO of 2.56–6.01%, MgO of 1.08–1.87% and K_2O of 1.59–3.55%. They plot in the trondhjemite and granodiorite fields (Fig. 8a) and show large variations in total rare earth elements (ΣREEs) (67–334 ppm), $(\text{La}/\text{Yb})_n$ (11.8–32.1) and Eu/Eu^* (0.6–1.3) (Fig. 9a, c). Compared with the TTG gneiss, the quartz monzonite and monzogranite gneiss samples (Fig. 8a) are higher in SiO_2 (68.29–73.77%) and K_2O (3.77–4.82%) and lower in TFeO

Fig. 6. (Colour online) $\epsilon_{\text{Hf}}(t)$ versus zircon age diagram for the late Neoproterozoic – early Palaeoproterozoic meta-plutonic rocks in the Daqingshan area, northwestern North China Craton. The weighted mean ^{207}Pb – ^{206}Pb age of 2500 Ma was used for samples with no magmatic zircon ages. Dotted and dashed lines represent felsic crust with $^{176}\text{Lu}/^{177}\text{Hf}$ being 0.01 and 0.015, respectively. CHUR – chondritic uniform reservoir.

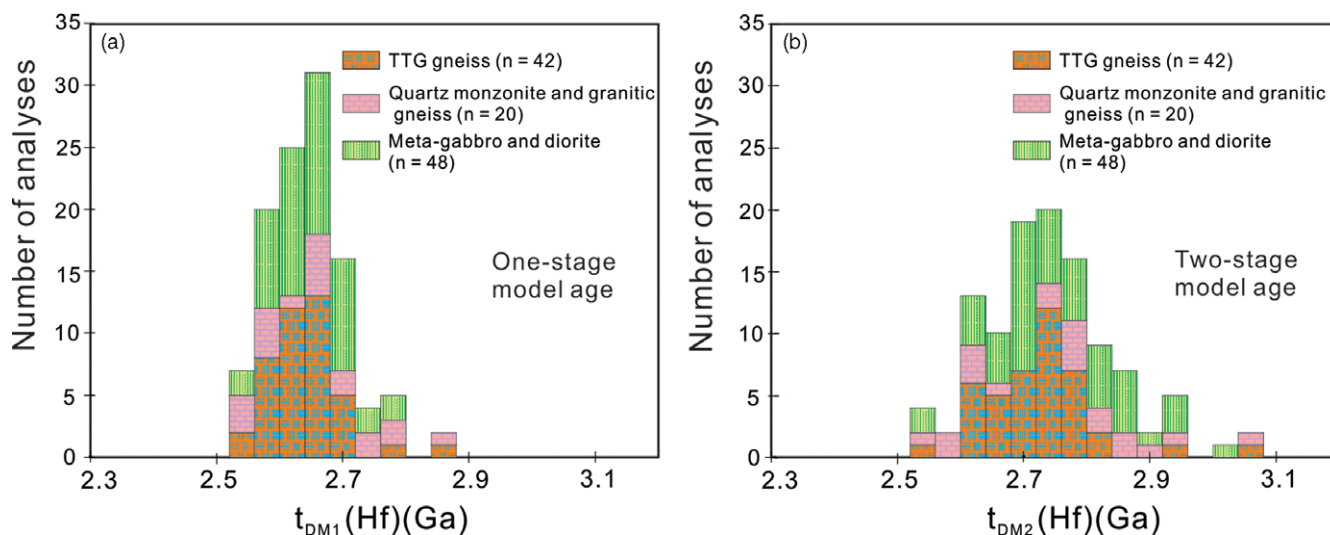
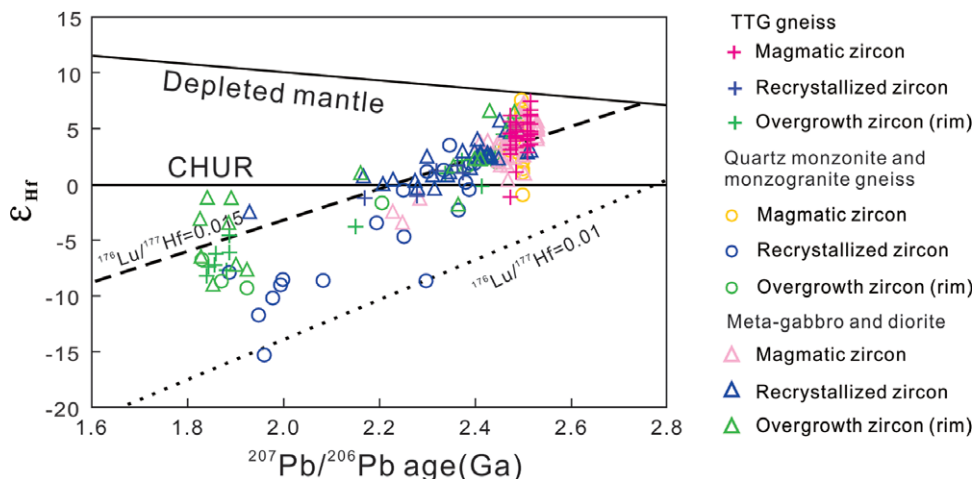


Fig. 7. (Colour online) Hf-in-zircon model age histograms for the late Neoproterozoic – early Palaeoproterozoic meta-plutonic rocks in the Daqingshan area, northwestern North China Craton. (a) One-stage model age; (b) two-stage model age.

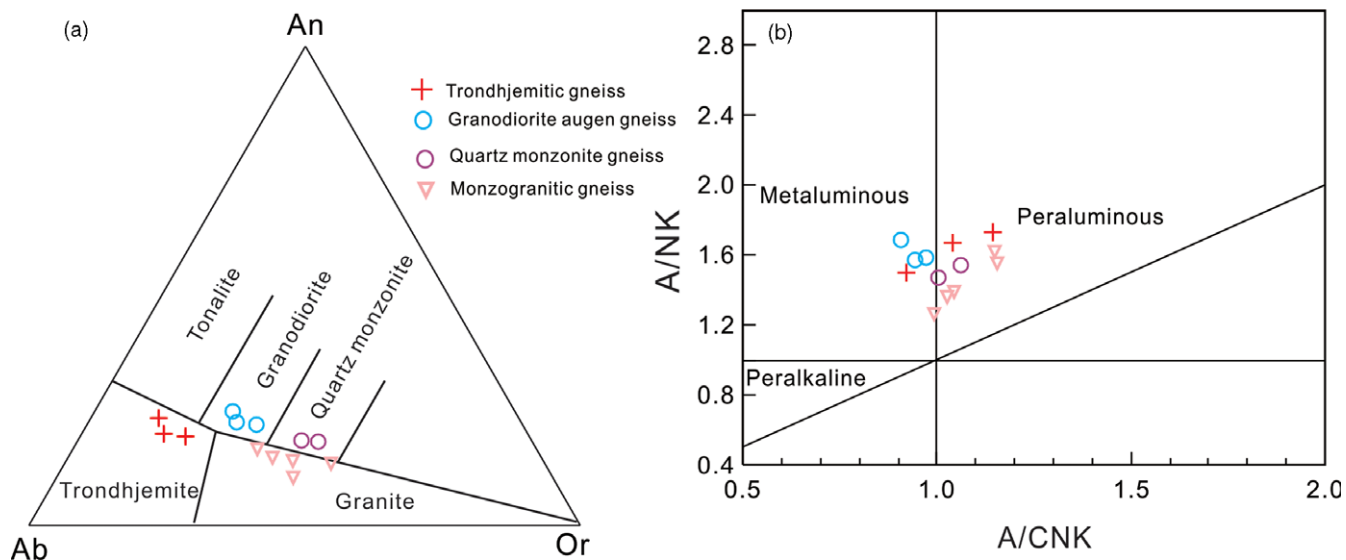


Fig. 8. (Colour online) (a) Modal An–Ab–Or and (b) A/CNK–A/NK diagrams of the late Neoproterozoic – early Palaeoproterozoic meta-plutonic rocks in the Daqingshan area, northwestern North China Craton.

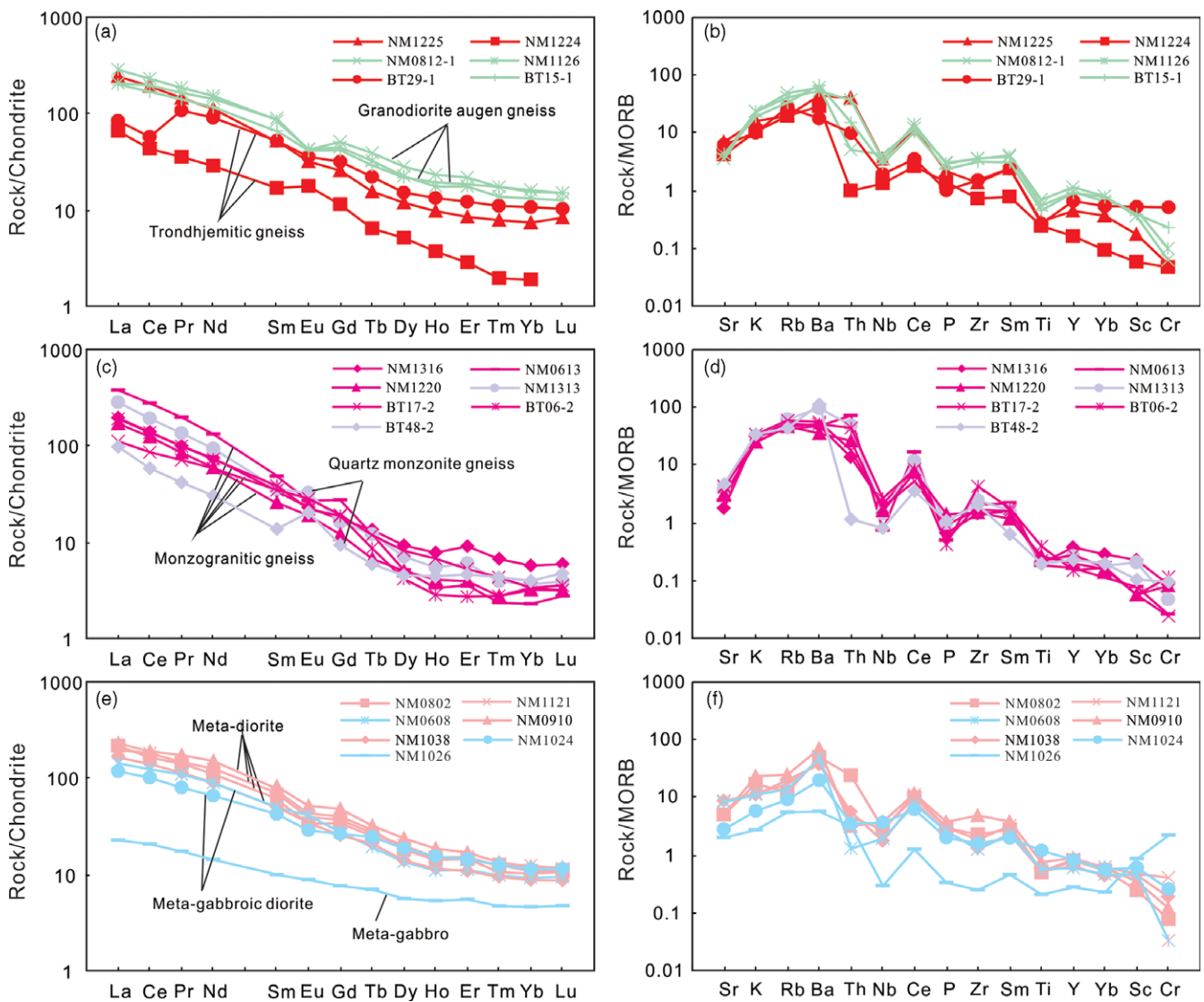


Fig. 9. (Colour online) REE and trace-element distribution patterns for the late Neoproterozoic – early Palaeoproterozoic meta-plutonic rocks in the Daqingshan area, northwestern North China Craton. (a, b) TTG; (c, d) monzogranite and quartz monzonite; (e, f) meta-gabbro and diorite. The samples with prefix BT are from Liu *et al.* (2017). Chondrite and primitive mantle normalization values are from Sun & McDonough (1989) and Pearce (1983), respectively.

(1.84–3.21 %) and MgO (0.20–1.39 %), have similar Σ REE contents (191–356 ppm) and Eu/Eu^* (0.72–1.3), but have larger $(\text{La}/\text{Yb})_n$ ratios (31.3–151.0; Fig. 9a, c). Most granitoids are peraluminous with some TTG being metaluminous (Fig. 8b). They are enriched in large ion lithophile elements (LILEs) and depleted in Nb and P (Fig. 9c, d).

The meta-gabbroic diorites and diorites (NM0608, NM0802, NM0910, NM1038, NM1024, NM1121) show inverse correlations of SiO_2 (53.98–59.62 %) with other oxides, including MgO (2.17–4.49 %), TFeO (5.99–10.68 %), CaO (4.65–7.82 %), Na_2O (3.62–4.66 %) and K_2O (0.87–3.48 %). They have similar REE patterns, with Σ REE, $(\text{La}/\text{Yb})_n$ and Eu^*/Eu being 153–296 ppm, 9.5–18.4 and 0.72–1.1, respectively (Fig. 9e). Meta-gabbro sample NM1026 has MgO = 12.93 %, TFeO = 7.45 %, Na_2O = 2.08 % and K_2O = 0.41 %. Compared with other meta-gabbroic diorites and diorites, it has a lower Σ REE content of 34 ppm and a lower $(\text{La}/\text{Yb})_n$ ratio of 4.5.

All the meta-gabbroic and dioritic rocks are enriched in LILEs and depleted in Nb (Fig. 9f).

7.b. Whole-rock Nd isotopes

A total of 11 samples, including three samples dated by Xu *et al.* (2015), were analysed for their Sm–Nd isotopic composition (online Supplementary Material Table S7). The TTG gneisses (NM0812-1, NM1126, NM1224, NM1225) are similar in their Nd isotopic compositions (Fig. 10). The $\epsilon_{\text{Nd}}(t)$, $t_{\text{DM1}}(\text{Nd})$ and $t_{\text{DM2}}(\text{Nd})$ values are +1.2 to +2.4, ~2.7 Ga and 2.8–2.7 Ga, respectively. The monzogranite gneiss (NM1220) is similar in Nd isotope composition to the TTG gneisses. The meta-gabbroic and dioritic rocks (NM0802, NM0910, NM1024, NM1026, NM1038, NM1121) are different in Nd isotopic compositions from the granitoid rocks, with the $\epsilon_{\text{Nd}}(t)$, $t_{\text{DM1}}(\text{Nd})$ and $t_{\text{DM2}}(\text{Nd})$ values being +1.5 to +4.3, 2.7–2.5 Ga and 2.8–2.6 Ga, respectively.

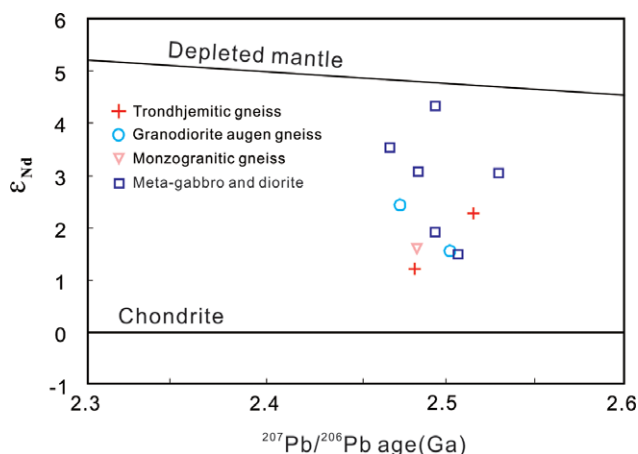


Fig. 10. (Colour online) Whole-rock $\epsilon_{Nd}(t)$ versus age diagram for the late Neoproterozoic – early Palaeoproterozoic meta-plutonic rocks in the Daqingshan area, northwestern North China Craton.

8. Discussion

8.a. Late Neoproterozoic – earliest Palaeoproterozoic magmatism

Among the 12 samples dated in this study, nine of them from a range of different rock types have the oldest population of magmatic zircons recording ages of 2530–2474 Ma (Table 2). Considering all samples, U–Pb zircon data recording both magmatic and metamorphic ages are distributed almost continuously along concordia from 2.53 Ga to 1.82 Ga. The oldest concordant magmatic zircons in the TTG samples range from 2516 ± 9 Ma to 2474 ± 12 Ma. Importantly, in some samples, zircon domains, interpreted as experiencing recrystallization, yield older ages than the magmatic cores. For example, in granodiorite augen gneiss sample NM0812-1, the recrystallized rim of grain 18 (18.1RC) has a ^{207}Pb – ^{206}Pb age of 2503 ± 15 Ma, older than the 2455 ± 9 Ma age of the magmatic core (18.2MA) (online Supplementary Material Table S4). Magmatic zircons from the quartz monzonite gneiss (NM1313) have the youngest magmatic ages of all the samples, ranging from 2391 Ma to 2188 Ma, but with one recrystallized rim (18.1R) recording an older age of 2402 ± 10 Ma (online Supplementary Material Table S4). For the monzogranite (NM0613), the two oldest analyses closest to concordia yield a weighted mean ^{207}Pb – ^{206}Pb age of 2497 ± 13 Ma, whereas the recrystallized domains record considerably younger ages ranging from 2314 ± 16 Ma to 1978 ± 30 Ma; note that no magmatic zircon domains remain in the mylonitized monzogranite sample NM1316. For the two diorite samples (NM0802, NM1121), the ages of the domains with magmatic structures range from 2538 ± 25 Ma to 2368 ± 37 Ma. Clearly, there are issues here with both a wide age range and such relatively young ages, suggesting that some oscillatory zoned domains have undergone radiogenic lead loss, while still retaining their ‘magmatic’ structure. This is also the case for the meta-gabbroic diorite (NM1024), where the oldest magmatic domain has an apparent age of 2471 ± 5 Ma, yet the oldest recrystallized domain has a similar ^{207}Pb – ^{206}Pb age of 2474 ± 12 Ma. The meta-gabbroic diorite NM0608 does not retain any magmatic domains, but the oldest recrystallized core records an apparent age of 2452 ± 27 Ma. The meta-gabbro (NM1026) records a maximum ^{207}Pb – ^{206}Pb age of 2520 ± 32 Ma from a magmatic domain, but with some

recrystallized cores being less than 50 Ma younger. In addition, many samples record late Palaeoproterozoic (1.95–1.82 Ga) ages, with their zircon data distributed along concordia, suggesting that they underwent strong overprinting by late Palaeoproterozoic events (e.g. meta-gabbroic diorite NM1024 and meta-diorite sample NM1121; see online Supplementary Material Table S4).

Dong *et al.* (2014) considered that the Daqingshan Supracrustal Rocks formed in earliest Palaeoproterozoic time based on the phenomenon that detrital magmatic zircons had apparent ages of 2.55–2.50 Ga and metamorphic zircon domains had apparent ages of 2.45–2.40 Ga. However, Zhang *et al.* (2016) established that they were deposited in late Neoproterozoic time owing to the supracrustal rocks being intruded by 2.5 Ga diorite. Indeed, in other areas of the NCC with evidence of both strong late Neoproterozoic and late Palaeoproterozoic tectonothermal events, such as in eastern Shandong and northwestern Hebei, it is common for the late widespread high-grade metamorphism to result in apparent younging of U–Pb ages in magmatic zircons due to recrystallization and ancient lead loss. Thus, such younger ages may not represent the time of zircon crystallization (even for those that still show good oscillatory zoning; Ma *et al.* 2012; Wan *et al.* 2020). This phenomenon has also been observed in mafic granulites in the Athabasca area, North America (Flowers *et al.* 2008).

Therefore, it is considered that most, if not all, rocks dated in this study were formed during late Neoproterozoic to earliest Palaeoproterozoic times (>2.48 Ga). Considering that the metamorphic zircon domains have complex structures and the samples analysed by LA-ICP-MS utilized a much greater volume of material than the SIMS U–Pb method, with the potential to traverse several different domains (Kröner *et al.* 2014), it is speculated that the ~2.45 Ga granitoid rocks dated by J. H. Liu *et al.* (2013, 2017) may also be late Neoproterozoic plutonic rocks. Therefore, major magmatism in the Daqingshan area mainly occurred in late Neoproterozoic – earliest Palaeoproterozoic times.

In the Daqingshan area, a series of tectonothermal events in late Palaeoproterozoic time caused high-grade metamorphism and deformation of the late Neoproterozoic K-rich granites. This is different from the Yinshan block in the north (inset in Fig. 1) where the late Palaeoproterozoic tectonothermal events were relatively weak, with most of the late Neoproterozoic meta-plutonic rocks having magmatic zircon ages >2500 Ma (e.g. Jian *et al.* 2012; Ma *et al.* 2013; Liu, J. H. *et al.* 2017; Dong *et al.* 2021). In these late Neoproterozoic gneisses, there are local middle to late Palaeoproterozoic plutonic rocks (Liu, J. H. *et al.* 2013; Liu, S. J. *et al.* 2013; Wan *et al.* 2013; Liu *et al.* 2014). However, in the Daqingshan area, most of the >1.85 Ga geological units are in tectonic contact, owing to the strong late Palaeoproterozoic tectonothermal events. The only exceptions are the latest Palaeoproterozoic red granites (mainly dykes), which intruded all earlier geological units.

The late Palaeoproterozoic tectonothermal events have long been widely recognized in the Daqingshan area (e.g. Ma *et al.* 2012; Dong *et al.* 2013; Liu, P. H. *et al.* 2017) and, indeed, throughout the Khondalite Belt (e.g. Jiao *et al.* 2020), resulting in final cratonization of the NCC (Zhai & Santosh, 2011) during amalgamation of the Columbia (Nuna) supercontinent (Rogers & Santosh, 2002; Zhao *et al.* 2002).

8.b. Petrogenesis of the plutonic rocks

Three types of rocks, including TTG, monzogranite and gabbro-diorite, have ‘magmatic’ zircon ages of ~2.5 Ga. The apparent ages

Table 2. Summary of zircon ages for the late Neoproterozoic – early Palaeoproterozoic meta-intrusive rocks in the Daqingshan area, northwestern North China Craton

No.	Sample no.	Rock type	Sample location	Magmatic zircon age (Ma)	Metamorphic zircon age (Ma)	Reference
1	NM1224	Trondhjemitic gneiss	~5 km northeast of Shaoniugou	2516 ± 9	1870 ± 11	this study
2	NM1225	Trondhjemitic gneiss	~2.5 km northeast of Shaoniugou	2483 ± 6	1844 ± 9	this study
3	BT29-1	Trondhjemitic gneiss	~12 km southeast of Shiguai	2470 ± 13	1904 ± 13	Liu <i>et al.</i> 2017
4	NM0812-1	Granodiorite augen gneiss	~3 km northeast of Hademengou	2474 ± 12	2503 ± 15/1856 ± 13 (n = 1)	this study
5	NM1126	Granodiorite augen gneiss	~2 km south of Shiguai	2510 ± 14	1956 ± 10 (n = 1)	this study
6	BT15-1	Granodioritic gneiss	~1 km southeast of Hujigou	2454 ± 7		Liu <i>et al.</i> 2017
7	NM1313	Quartz monzonite gneiss	~500 m south of Jiagenqigou		1887 ± 29 (n = 1)	this study
8	BT48-2	Quartz monzonite gneiss	~1 km north of Maohudong	2455 ± 15	1894 ± 39	Liu <i>et al.</i> 2017
9	NM1316	Mylonitized augen monzogranite	~200 m east of Jiagenqigou		1951 ± 7/1884 ± 19	this study
10	NM0613	Monzogranitic gneiss	~2 km northwest of Maohudong	2497 ± 13	1982 ± 35	this study
11	NM1220	Monzogranitic gneiss	~16 km southwest of Shiguai	2484 ± 7	2441 ± 7/1847 ± 35	Xu <i>et al.</i> 2015
12	BT06-2	Monzogranitic gneiss	~6 km northwest of Hademengou	2459 ± 7	2456 ± 7	Liu <i>et al.</i> 2017
13	BT17-2	Monzogranitic gneiss	~12 km south of Hujigou	2430 ± 8	1936 ± 20	Liu <i>et al.</i> 2017
14	NM0802	Meta-diorite	~1 km west of Hujigou	2530 ± 28	1833 ± 32	this study
15	NM1121	Meta-diorite	~3 km east of Hujigou	2495 ± 28		this study
16	NM1026	Meta-gabbro	~2 km northeast of Hademengou	2502 ± 28	1841 ± 4 (n = 1)	this study
17	NM0910	Meta-diorite	~7 km south of Shiguai	2494 ± 12	1919 ± 73	Xu <i>et al.</i> 2015
18	NM1038	Meta-diorite	~13 km southeast of Shiguai	2495 ± 10	2481 ± 10	Xu <i>et al.</i> 2015
19	NM0608	Meta-gabbroic diorite	~3 km southwest of Taoerwan		1887 ± 80	this study
20	NM1024	Meta-gabbroic diorite	~6 km northeast of Hademengou	2469 ± 7		this study

cannot be used to determine their formation order owing to strong late Palaeoproterozoic tectonothermal overprinting, which resulted in ancient lead loss of magmatic zircon. However, field observation suggests that the gabbro-diorite commonly formed slightly later than the TTG rocks, and the monzogranite was younger than the TTG rocks.

The various plutonic rock types in this study are similar in composition to those described by J. H. Liu *et al.* (2017) (Figs 8, 9, 11, 12). The TTG rocks commonly have low Sr/Y and La/Yb ratios (Fig. 11a, b), indicating that they formed by partial melting of basaltic rocks under low- to medium-pressure conditions where garnet is absent, but plagioclase is residual (Rapp & Watson, 1995; Moyen, 2011). Quartz monzonitic and monzogranitic gneisses are richer in K₂O and show higher La/Yb ratios compared with the TTG rocks. It is notable that quartz monzonite sample NM1313 has a SiO₂ content of 68.29 wt %, being higher than the TTG rocks; thus, sample NM1313 is likely to be granite rather than quartz monzonite. However, considering the anatexis and strong deformation, the high SiO₂ content may be due to local migration of material. The monzogranites may be derived from

recycling of continental material or magma mixing, and their composition mainly reflects that of their source region. The meta-gabbroic and dioritic rocks are high in ΣREEs and show REE fractionation, suggesting that they were derived from enriched mantle, and that assimilation–fractional crystallization (AFC) processes may play an important role in their formation. The mafic to intermediate magmatism not only added material to the continental crust but also provided heat for formation of crustally derived granites in an extensional environment.

The TTG gneisses have whole-rock $\epsilon_{Nd}(t)$ of +1.2 to +2.4 (Fig. 10) and $t_{DM1}(Nd)$ of 2.7 Ga, whereas analyses on magmatic zircons from the TTG gneisses have $\epsilon_{Hf}(t)$ values of –1.1 to +6.2 and $t_{DM1}(Hf)$ of 2.7–2.5 Ga (Figs 6, 7a). These indicate that the TTG rocks were derived from mafic material input from the mantle at ~2.5 Ga or slightly earlier. Considering the absence of zircon >2.6 Ga, the Sanggan Group may have formed in an oceanic environment, whereas the TTG rocks formed as a result of partial melting of the basaltic rocks (oceanic crust?) of the Sanggan Group under relatively low-pressure conditions. The quartz monzonite and monzogranite gneisses are similar in Nd–Hf isotope

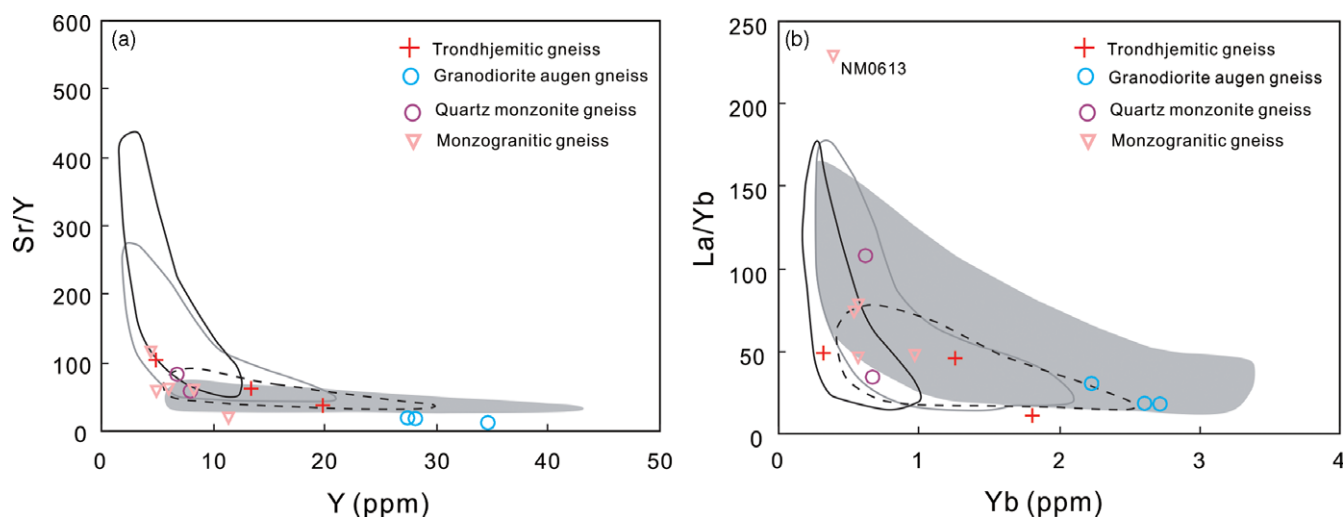


Fig. 11. (Colour online) (a) Sr/Y–Y and (b) La/Yb–Yb diagrams (after Moyen, 2011) for the late Neoarchaeon – early Palaeoproterozoic meta-plutonic granitoids in the Daqingshan area, northwestern North China Craton. The marked fields are as follows: grey shaded area – potassic granitoids; within thick black line – high-pressure TTG; within grey line – medium-pressure TTG; within dashed line – low-pressure TTG.

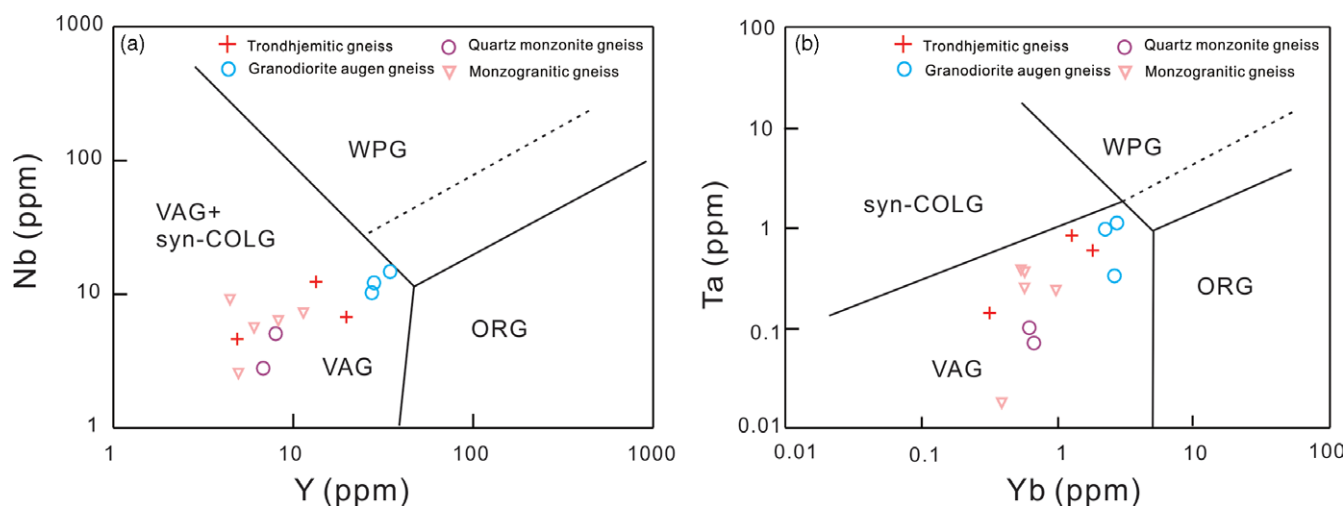


Fig. 12. (Colour online) (a) Nb–Y and (b) Ta–Yb diagrams (after Pearce *et al.* 1984) for the late Neoarchaeon – early Palaeoproterozoic meta-plutonic granitoids in the Daqingshan area, northwestern North China Craton. syn-COLG – syn-collision granites; VAG – volcanic arc granites; WPG – within plate granites; ORG – ocean ridge granites. The dashed line represents the upper compositional boundary for ORG from anomalous ridge segments.

composition to the TTG gneisses. This suggests that they were influenced by, or partially derived from, Neoarchaeon continental basement. The gabbroic and dioritic rocks are similar in Nd–Hf isotopic composition to the granitoid gneisses, but with derivation from enriched mantle accompanied by AFC processes, as revealed by their element compositions. Overall, the Nd–Hf isotope compositions of the rocks are similar to those of the late Neoarchaeon rocks all over the NCC, consistent with the view that the late Mesoarchaeon – early Neoarchaeon was an important period when much of the NCC (and global) juvenile continental crust formed (Condie, 2000; Condie *et al.* 2009; Geng *et al.* 2012; Wan *et al.* 2015).

8.c. Tectonic environment in the late Neoarchaeon

There are different opinions on whether mantle plume activity (or underplating) and/or arc magmatism, or both, played key roles in the Neoarchaeon period (Chadwick *et al.* 2007; Condie & Kröner,

2013; Mohan *et al.* 2013), and the same applies to the NCC (Zhao *et al.* 2001; Kusky & Li, 2003; Kröner *et al.* 2005; Wilde *et al.* 2005; Geng *et al.* 2006; Yang *et al.* 2008; Liu *et al.* 2011; Nutman *et al.* 2011). In the Daqingshan area, the late Neoarchaeon Sanggan Group is mainly composed of mesocratic and leucocratic granulite units, whose protoliths were considered to be mainly basaltic and andesitic rocks, respectively (Yang *et al.* 2003, 2006). From the perspective of regional structure, Yang *et al.* (2003, 2006) indicated that the original Upper Wulashan Group (including the Daqingshan Supracrustal Rocks) formed later than the Sanggan Group. It is notable that in the Daqingshan area, no rock >2.6 Ga has been identified, and zircon >2.6 Ga is absent or rare in any type of rocks. This is different from many other areas of the NCC. The late Neoarchaeon granitoid rocks from the Daqingshan area plot in the volcanic arc granites (VAG) + syn-collision granites (syn-COLG) field in the Nb–Y diagram (Fig. 12a) and in the VAG field in the Ta–Yb diagram (Fig. 12b). All rocks, including the meta-gabbroic and dioritic rocks, show LILE enrichment and Nb

depletion in their trace-element distribution patterns (Fig. 9b, d, f). Depletion of Th in some samples may be due to the influence of the strong Palaeoproterozoic tectonothermal events. Therefore, this study supports the conclusion of J. H. Liu *et al.* (2017) that the late Neoproterozoic plutonic rocks in the Daqingshan area formed as a result of arc magmatism. We further suggest that it may be an intra-oceanic arc environment, rather than an Andean-type arc environment in terms of the rock association of the Sanggan Group (mainly meta-basaltic and andesitic rocks) and the absence of >2.6 Ga rocks and zircons.

9. Conclusions

- (1) Late Neoproterozoic magmatism was well developed in the Daqingshan area, probably extending into earliest Palaeoproterozoic time. The rock types include TTG, quartz monzonite, monzogranite and gabbroic and dioritic rocks.
- (2) The TTG gneisses have low Sr/Y and La/Yb ratios, and have whole-rock $\epsilon_{\text{Nd}}(t)$ and magmatic zircon $\epsilon_{\text{Hf}}(t)$ values of +1.2 to +2.4 and -1.1 to +6.2, respectively. The quartz monzonite and monzogranite gneisses are similar in Nd–Hf isotope composition to the TTG gneisses. The gabbroic and dioritic rocks are high in ΣREEs and show REE fractionation, but have similar Nd–Hf isotopic compositions to the granitoids.
- (3) As in many other areas of the NCC and worldwide, the late Mesoproterozoic – early Neoproterozoic was an important period when huge volumes of continental crust formed. The Daqingshan area may have been an intra-oceanic arc environment, rather than an Andean-type arc environment during the late Neoproterozoic period.
- (4) Most of the Neoproterozoic rocks in the Daqingshan area underwent strong tectonothermal events in late Palaeoproterozoic time. These events were widespread in the NCC, resulting in the final cratonization of the NCC.

Supplementary material. To view supplementary material for this article, please visit <https://doi.org/10.1017/S0016756822001212>

Acknowledgements. We express our gratitude to Weilin Gan for making the zircon mounts; Xiaochao Che and Jianhui Liu are thanked for maintenance of the SHRIMP II, and Liqin Zhou and Zhichao Zhang for help with CL imaging. We are grateful to editor Tim Johnson and two anonymous reviewers for their valuable comments and suggestions. The study was supported financially by the National Natural Science Foundation of China [41472167, 41872200].

References

- Black LP, Kamo SL, Allen CM, Aleinikoff JK, Davis DW, Korsch RJ and Foudoulis C (2003) TEMORA 1: a new zircon standard for Phanerozoic U–Pb geochronology. *Chemical Geology* **200**, 155–70. doi: [10.1016/S0009-2541\(03\)00165-7](https://doi.org/10.1016/S0009-2541(03)00165-7).
- Bouvier A, Vervoort JD and Patchett PJ (2008) The Lu–Hf and Sm–Nd isotopic composition of CHUR: constraints from unequilibrated chondrites and implications for the bulk composition of terrestrial planets. *Earth and Planetary Science Letters* **273**, 48–57. doi: [10.1016/j.epsl.2008.06.010](https://doi.org/10.1016/j.epsl.2008.06.010).
- Cai J, Liu FL, Liu PH, Wang F, Liu CH and Shi JR (2014) Metamorphic P–T path and tectonic implications of pelitic granulites from the Daqingshan Complex of the Khondalite Belt, North China Craton. *Precambrian Research* **241**, 161–81. doi: [10.1016/j.precamres.2013.11.012](https://doi.org/10.1016/j.precamres.2013.11.012).
- Chadwick B, Vasudev VN, Hegde GV and Nutman AP (2007) Structure and SHRIMP U/Pb zircon ages of granites adjacent to the Chitradurga Schist Belt: implications for Neoproterozoic convergence in the Dharwar Craton, southern India. *Journal of the Geological Society of India* **69**, 5–24.
- Condie KC (2000) Episodic continental growth models: afterthoughts and extensions. *Tectonophysics* **322**, 153–62. doi: [10.1016/S0040-1951\(00\)00061-5](https://doi.org/10.1016/S0040-1951(00)00061-5).
- Condie KC, Belousova E, Griffin WL and Sircombe KN (2009) Granitoid events in space and time: constraints from igneous and detrital zircon age spectra. *Gondwana Research* **15**, 228–42. doi: [10.1016/j.gr.2008.06.001](https://doi.org/10.1016/j.gr.2008.06.001).
- Condie KC and Kröner A (2013) The building blocks of continental crust: evidence for a major change in the tectonic setting of continental growth at the end of the Archean. *Gondwana Research* **23**, 394–402. doi: [10.1016/j.gr.2011.09.011](https://doi.org/10.1016/j.gr.2011.09.011).
- Cumming GL and Richards JR (1975) Ore lead isotope ratios in a continuously changing earth. *Earth and Planetary Science Letters* **28**, 155–71. doi: [10.1016/0012-821X\(75\)90223-X](https://doi.org/10.1016/0012-821X(75)90223-X).
- DePaolo DJ (1988) Age dependence of the composition of continental crust: evidence from Nd isotopic variations in granitic rocks. *Earth and Planetary Science Letters* **90**, 263–71. doi: [10.1016/0012-821X\(88\)90130-6](https://doi.org/10.1016/0012-821X(88)90130-6).
- Dong CY, Ma MZ, Wilde SA, Liu SJ, Li PC, Xu ZY, Wan YS (2022) The first identification of early Paleoproterozoic (2.46–2.38 Ga) supracrustal rocks in the Daqingshan area, northwestern North China Craton: geology, geochemistry and SHRIMP U–Pb dating. *Gondwana Research* **37**, 106727. doi: [10.1016/j.precamres.2022.106727](https://doi.org/10.1016/j.precamres.2022.106727).
- Dong CY, Ma MZ, Xie HQ, Zhang YX and Wan YS (2021) Magmatism and metamorphism of the early Precambrian basement in the Bayan Obo area, Inner Mongolia: zircon SHRIMP U–Pb dating and LA–MC–ICPMS Hf analysis. *Acta Petrologica Sinica* **37**, 417–32 (in Chinese with English abstract).
- Dong CY, Wan YS, Wilde SA, Xu ZY, Ma MZ, Xie HQ and Liu DY (2014) Earliest Paleoproterozoic supracrustal rocks in the North China Craton recognized from the Daqingshan area of the Khondalite Belt: constraints on craton evolution. *Gondwana Research* **25**, 1535–53. doi: [10.1016/j.gr.2013.05.021](https://doi.org/10.1016/j.gr.2013.05.021).
- Dong CY, Wan YS, Xu ZY and Liu DY (2013) SHRIMP zircon U–Pb dating of late Paleoproterozoic kandalites in the Daqing Mountains area on the North China Craton. *Science in China Earth Sciences* **56**, 115–25. doi: [10.1007/s11430-012-4459-3](https://doi.org/10.1007/s11430-012-4459-3).
- Ehllou S, Belousova E, Griffin WL, Pearson NJ and O'Reilly SY (2006) Trace element and isotopic composition of GJ red zircon standard by laser ablation. *Geochimica et Cosmochimica Acta* **70**, A158. doi: [10.1016/j.gca.2006.06.1383](https://doi.org/10.1016/j.gca.2006.06.1383).
- Flowers RM, Bowring SA, Mahan KH, Williams ML and Williams IS (2008) Stabilization and reactivation of cratonic lithosphere from the lower crustal record in the Western Canadian Shield. *Contributions to Mineralogy and Petrology* **156**, 529–49. doi: [10.1007/s00410-008-0301-5](https://doi.org/10.1007/s00410-008-0301-5).
- Geng YS, Du LL and Ren LD (2012) Growth and reworking of the early Precambrian continental crust in the North China Craton: constraints from zircon Hf isotopes. *Gondwana Research* **21**, 517–29. doi: [10.1016/j.gr.2011.07.006](https://doi.org/10.1016/j.gr.2011.07.006).
- Geng YS, Liu FL and Yang CH (2006) Magmatic event at the end of the Archean in eastern Hebei Province and its geological implication. *Acta Geologica Sinica* **80**, 819–33. doi: [CNKI:SUN:DZXW.0.2006-06-003](https://doi.org/CNKI:SUN:DZXW.0.2006-06-003) (in Chinese with English abstract).
- Griffin WL, Wang X, Jackson SE, Pearson SE, O'Reilly SY, Xu XS and Zhou XM (2002) Zircon chemistry and magma genesis, SE China: in-situ analysis of Hf isotopes, Tonglu and Pingtan igneous complexes. *Lithos* **61**, 237–69. doi: [10.1016/S0024-4937\(02\)00082-8](https://doi.org/10.1016/S0024-4937(02)00082-8).
- Hou KJ, Li YH, Zou TR, Shi YR and Xie GQ (2007) Laser ablation MC–ICP–MS technique for Hf isotope microanalysis of zircon and its geological applications. *Acta Petrologica Sinica* **23**, 2595–604. doi: [10.1631/jzus.2007.B0900](https://doi.org/10.1631/jzus.2007.B0900) (in Chinese with English abstract).
- Jian P, Kröner A, Windley BF, Zhang Q, Zhang W and Zhang LQ (2012) Episodic mantle melting–crustal reworking in the late Neoproterozoic of the northwestern North China Craton: zircon ages of magmatic and metamorphic rocks from the Yinshan Block. *Precambrian Research* **222–223**, 230–54.
- Jiao SJ, Fitzsimons ICW, Zi JW, Evans NJ, McDonald BJ and Guo JH (2020) Texturally controlled U–Th–Pb monazite geochronology reveals Paleoproterozoic UHT metamorphic evolution in the Khondalite Belt North China Craton. *Journal of Petrology* **61**, ega023. doi: [10.1093/petrology/egaa023](https://doi.org/10.1093/petrology/egaa023).

- Jin W, Li SX and Liu XS** (1991) A study on characteristics of Early Precambrian high-grade metamorphic rock series and their metamorphic dynamics. *Acta Petrologica Sinica* **4**, 27–35 (in Chinese with English abstract).
- Jin W, Li SX and Liu XS** (1992) Early Precambrian metamorphic rocks and early earth crust evolution in Daqingshan, Inner Mongolia. *Journal of Changchun University (Earth Science Edition)* **22**, 281–9 (in Chinese with English abstract).
- Kröner A, Wan YS, Liu XM and Liu DY** (2014) Dating of zircon from high-grade rocks: which is the most reliable method?. *Geoscience Frontiers* **5**, 515–23. doi: [10.1016/j.gsf.2014.03.012](https://doi.org/10.1016/j.gsf.2014.03.012).
- Kröner A, Wilde SA, Li JH and Wang KY** (2005) Age and evolution of a late Archean to Paleoproterozoic upper to lower crustal section in the Wutaishan/Hengshan/Fuping terrain of northern China. *Journal of Asian Earth Sciences* **24**, 577–95. doi: [10.1016/j.jseas.2004.01.001](https://doi.org/10.1016/j.jseas.2004.01.001).
- Kusky TM and Li JH** (2003) Paleoproterozoic tectonic evolution of the North China Craton. *Journal of Asian Earth Sciences* **22**, 383–97. doi: [10.1016/S1367-9120\(03\)00071-3](https://doi.org/10.1016/S1367-9120(03)00071-3).
- Li PC, Wan YS, Xie HQ, Wilde SA and Liu DY** (2022) Geology of the 2022 Winter Olympic sites, Beijing-Zhangjiakou, China: an analogue of the North China Craton. *International Geology Review* **64**, 2890–921. doi: [10.1080/00206814.2021.2007507](https://doi.org/10.1080/00206814.2021.2007507).
- Liu SJ, Dong CY, Xu ZY, Santosh M, Ma MZ, Xie HQ, Liu DY and Wan YS** (2013) Palaeoproterozoic episodic magmatism and high-grade metamorphism in the North China Craton: evidence from SHRIMP zircon dating of magmatic suites in the Daqingshan area. *Geological Journal* **48**, 429–55. doi: [10.1002/gj.2453](https://doi.org/10.1002/gj.2453).
- Liu PH, Liu FL, Cai J, Liu CH, Liu JH, Wang F, Xiao LL and Shi JR** (2017) Spatial distribution, P-T-t paths, and tectonic significance of high-pressure mafic granulites from the Daqingshan-Wulashan Complex in the Khondalite Belt, North China Craton. *Precambrian Research* **303**, 687–708. doi: [10.1016/j.precamres.2017.09.004](https://doi.org/10.1016/j.precamres.2017.09.004).
- Liu JH, Liu FL, Ding ZJ, Chen JQ, Liu PH, Shi JR, Cai J and Wang F** (2013) Zircon U-Pb chronology, geochemistry and their petrogenesis of Early Paleoproterozoic granitoid gneisses in Ulashan area, North China Craton. *Acta Petrologica Sinica* **29**, 485–500. doi: [10.1016/j.sedgeo.2012.12.001](https://doi.org/10.1016/j.sedgeo.2012.12.001) (in Chinese with English abstract).
- Liu JH, Liu FL, Ding ZJ, Liu PH, Chen JQ, Liu CH, Wang F, Yang H, Cai J and Shi JR** (2017) Late Neoproterozoic–Paleoproterozoic arc-continent accretion along the Khondalite Belt, Western Block, North China Craton: insights from granitoid rocks of the Daqingshan-Wulashan area. *Precambrian Research* **303**, 494–519. doi: [10.1016/j.precamres.2017.06.006](https://doi.org/10.1016/j.precamres.2017.06.006).
- Liu PH, Liu FL, Liu CH, Liu JH, Wang F, Xiao LL, Cai J and Shi JR** (2014) Multiple mafic magmatic and high-grade metamorphic events revealed by zircons from meta-mafic rocks in the Daqingshan–Wulashan Complex of the Khondalite Belt, North China Craton. *Precambrian Research* **246**, 34–357. doi: [10.1016/j.precamres.2014.02.015](https://doi.org/10.1016/j.precamres.2014.02.015).
- Liu DY, Nutman AP, Compston W, Wu JS and Shen QH** (1992) Remnants of 3800 Ma crust in the Chinese part of the Sino-Korean Craton. *Geology* **20**, 339–42. doi: [10.1130/0091-7613\(1992\)020<0339:ROMCIT>2.3.CO;2](https://doi.org/10.1130/0091-7613(1992)020<0339:ROMCIT>2.3.CO;2).
- Liu SW, Santosh M, Wang W, Bai X and Yang PT** (2011) Zircon U-Pb chronology of Jianping Complex: implications for the Precambrian crustal evolution history of the northern margin of the North China Craton. *Gondwana Research* **20**, 48–63. doi: [10.1016/j.gr.2011.01.003](https://doi.org/10.1016/j.gr.2011.01.003).
- Ludwig KR** (2001) *Isoplot/ex(rev). 2.49: A Geochronological Toolkit for Microsoft Excel*. Berkeley Geochronological Center, Special Publication no. 1a.
- Ludwig KR** (2003) *User's Manual for Isoplot 3.00: A Geochronological Toolkit for Microsoft Excel*. Berkeley Geochronology Center, Special Publication no. 4.
- Ma XD, Fan HR and Guo JH** (2013) Neoproterozoic magmatism, metamorphism in the Yinshan Block: implication for the genesis of BIF and crustal evolution. *Acta Petrologica Sinica* **29**, 2329–39.
- Ma MZ, Wan YS, Santosh M, Xu ZY, Xie HQ, Dong CY, Liu DY and Guo CL** (2012) Decoding multiple tectonothermal events in zircons from single rock samples: SHRIMP zircon U-Pb data from the late Neoproterozoic rocks of Daqingshan, North China Craton. *Gondwana Research* **22**, 810–27. doi: [10.1016/j.gr.2012.02.020](https://doi.org/10.1016/j.gr.2012.02.020).
- Mohan MR, Piercy SJ, Kamber BS and Sarma DS** (2013) Subduction related tectonic evolution of the Neoproterozoic eastern Dharwar Craton, southern India: new geochemical and isotopic constraints. *Precambrian Research* **227**, 204–26. doi: [10.1016/j.precamres.2012.06.012](https://doi.org/10.1016/j.precamres.2012.06.012).
- Moyen JF** (2011) The composite Archean grey gneisses: petrological significance, and evidence for a non-unique tectonic setting for Archean crustal growth. *Lithos* **123**, 21–36. doi: [10.1016/j.lithos.2010.09.015](https://doi.org/10.1016/j.lithos.2010.09.015).
- Nasdala L, Hofmeister W, Norberg N, Mattinson JM, Corfu F, Dor W, Kamo SL, Allen K, Kennedy AK, Kronz A, Reiners PW, Frei D, Kosler J, Wan YS, Goze J, Hoer T, Kröner A and Valley JW** (2008) Zircon M257—a homogeneous natural reference material for the ion microprobe U-Pb analysis of zircon. *Geostandards and Geoanalytical Research* **32**, 247–65. doi: [10.1111/j.1751-908X.2008.00914.x](https://doi.org/10.1111/j.1751-908X.2008.00914.x).
- Nutman AP, Wan YS, Du LL, Friend CRL, Dong CY, Xie HQ, Wang W, Sun HY and Liu DY** (2011) Multistage late Neoproterozoic crustal evolution of the North China Craton, eastern Hebei. *Precambrian Research* **189**, 43–65. doi: [10.1016/j.precamres.2011.04.005](https://doi.org/10.1016/j.precamres.2011.04.005).
- Pearce JA** (1983) Role of the subcontinental lithosphere in magma genesis at active continental margins. In *Continental Basalts and Mantle Xenoliths* (eds CJ Hawkesworth and MJ Norry), pp. 230–49. Nantwich, UK: Shiva Publishing Ltd.
- Pearce JA, Harris NBW and Tindle AG** (1984) Trace element discrimination diagrams for the tectonic interpretation of granitic rocks. *Journal of Petrology* **25**, 956–83. doi: [10.1093/petrology/25.4.956](https://doi.org/10.1093/petrology/25.4.956).
- Rapp RP and Watson EB** (1995) Dehydration melting of metabasalt at 8–32 kbar: implications for continental growth and crust-mantle recycling. *Journal of Petrology* **36**, 891–931. doi: [10.1093/petrology/36.4.891](https://doi.org/10.1093/petrology/36.4.891).
- Rogers JJW and Santosh M** (2002) Configuration of Columbia, a Mesoproterozoic supercontinent. *Gondwana Research* **5**, 5–22.
- Shi Q, Ding D, Xu ZY, Li WQ, Li G, Li CX, Zhao ZH, Zhang GB, Jiang XY, Yang RB and Zhou ZY** (2021) Metamorphic evolution of Daqingshan supracrustal rocks and garnet granite from the North China Craton: constraints from phase equilibria modelling, geochemistry, and SHRIMP U-Pb geochronology. *Gondwana Research* **97**, 101–20. doi: [10.1016/j.gr.2021.05.014](https://doi.org/10.1016/j.gr.2021.05.014).
- Söderlund U, Patchett PJ, Vervoort JD and Isachsen CE** (2004) The ¹⁷⁶Lu decay constant determined by Lu-Hf and U-Pb isotope systematics of Precambrian mafic intrusions. *Earth and Planetary Science Letters* **219**, 311–24. doi: [10.1016/S0012-821X\(04\)00012-3](https://doi.org/10.1016/S0012-821X(04)00012-3).
- Sun SS and McDonough WF** (1989) Chemical and isotopic systematics of oceanic basalts: implications for mantle composition and processes. In *Magmatism in the Ocean Basins* (eds AD Saunders and MJ Norry), pp. 313–45. Geological Society of London, Special Publication no. 42.
- Wan YS, Liu DY, Dong CY, Xie HQ, Kröner A, Ma MZ, Liu SJ, Xie SW and Ren P** (2015) Formation and evolution of Archean continental crust of the North China Craton. In *Precambrian Geology of China* (ed. MG Zhai), pp. 59–136. Berlin, Heidelberg: Springer-Verlag.
- Wan YS, Liu DY, Dong CY, Xu ZY, Wang ZJ, Wilde SA, Yang YH, Liu ZH and Zhou HY** (2009) The Precambrian Khondalite Belt in the Daqingshan area, North China Craton: evidence for multiple metamorphic events in the Palaeoproterozoic era. In *Palaeproterozoic Supercontinents and Global Evolution* (eds SM Reddy, R Mazumder, DAD Evans and AS Collins), pp. 73–97. Geological Society, London Special Publication no. 323. doi: [10.1144/SP323.4](https://doi.org/10.1144/SP323.4).
- Wan YS, Xie HQ, Dong CY and Liu DY** (2020) Timing of tectonothermal events in Archean basement of the North China Craton. *Earth Science* **45**, 3119–60. doi: [10.3799/dqkx.2020.121](https://doi.org/10.3799/dqkx.2020.121) (in Chinese with English abstract).
- Wan YS, Xie HQ, Wang HC, Liu SJ, Chu H, Xiao ZB, Li Y, Hao GM, Li PC, Dong CY and Liu DY** (2021) Discovery of early Eoarchean-Hadean zircons in eastern Hebei, North China Craton. *Acta Geologica Sinica* **95**, 277–91 (in Chinese with English abstract).
- Wan YS, Xu ZY, Dong CY, Nutman A, Ma MZ, Xie HQ, Liu SJ, Liu DY, Wang HC and Chu H** (2013) Episodic Paleoproterozoic (~2.45, ~1.95 and ~1.85 Ga) mafic magmatism and associated high temperature metamorphism in the Daqingshan area, North China Craton: SHRIMP zircon U-Pb dating and whole-rock geochemistry. *Precambrian Research* **224**, 71–93. doi: [10.1016/j.precamres.2012.09.014](https://doi.org/10.1016/j.precamres.2012.09.014).

- Wilde SA, Cawood PA, Wang KY and Nemchin AA** (2005) Granitoid evolution in the Late Archean Wutai Complex, North China Craton. *Journal of Asian Earth Sciences* **24**, 597–613. doi: [10.1016/j.jseae.2003.11.006](https://doi.org/10.1016/j.jseae.2003.11.006).
- Williams IS** (1998) U-Th-Pb geochronology by ion microprobe. In *Applications of Microanalytical Techniques to Understanding Mineralizing Processes* (eds MA McKibben, WC Shanks and WI Ridley), pp. 1–35. Reviews in Economic Geology vol. 7. Littleton CO: Society of Economic Geologists.
- Woodhead JD and Hergt JM** (2005) Preliminary appraisal of seven natural zircon reference materials for in situ Hf isotope determination. *Geostandards and Geoanalytical Research* **29**, 183–95.
- Xu ZY, Liu ZH, Hu FX and Yang ZS** (2005) Geochemical characteristics of the calc-silicate rocks in khondalite series in Daqingshan area, Inner Mongolia. *Journal of Jilin University (Earth Science Edition)* **35**, 681–9 (in Chinese with English abstract).
- Xu ZY, Liu ZH and Yang ZS** (2002) The strata texture of khondalite in Daqingshan area, Inner Mongolia. *Journal of Jilin University (Earth Science Edition)* **32**, 313–18. doi: [10.1080/12265080208422884](https://doi.org/10.1080/12265080208422884) (in Chinese with English abstract).
- Xu ZY, Liu ZH, Yang ZS, Wu XW and Chen XF** (2007) Structure of metamorphic strata of the khondalite series in the Daqingshan-Wulashan area, central Inner Mongolia, China, and their geodynamic implications. *Geological Bulletin of China* **26**, 526–36. doi: [10.1016/S1872-5791\(07\)60044-X](https://doi.org/10.1016/S1872-5791(07)60044-X) (in Chinese with English abstract).
- Xu ZY, Wan YS, Dong CY, Ma MZ and Liu DY** (2015) Late Neoproterozoic magmatism identified in Daqingshan, Inner Mongolia: SHRIMP zircon U-Pb dating. *Acta Petrologica Sinica* **31**, 1509–17 (in Chinese with English abstract).
- Yang JH, Wu FY, Wilde SA and Zhao GC** (2008) Petrogenesis and geodynamics of Late Archean magmatism in eastern Hebei, eastern North China Craton: geochronological, geochemical and Nd-Hf isotopic evidence. *Precambrian Research* **167**, 125–49. doi: [10.1016/j.precamres.2008.07.004](https://doi.org/10.1016/j.precamres.2008.07.004).
- Yang ZS, Xu ZY and Liu ZH** (2003) Consideration and practice of the construction of lithostratigraphic system in high-grade metamorphic terrains – a case study in the Daqingshan-Wulashan area. *Geology in China* **30**, 343–51 (in Chinese with English abstract).
- Yang ZS, Xu ZY, Liu ZH and Huang DL** (2006) Major progress in Early Precambrian research in the Daqing Shan-Wula Shan region, central Inner Mongolia, China, and some suggestions for stratigraphic work in high-grade metamorphic areas. *Geological Bulletin of China* **25**, 427–33 (in Chinese with English abstract).
- Yuan HL, Gao S, Dai MN, Zong CL, Günther D, Fontaine GH, Liu XM and Diwu CR** (2008) Simultaneous determinations of U-Pb age, Hf isotopes and trace element compositions of zircon by excimer laser-ablation quadrupole and multiple-collector ICP-MS. *Chemical Geology* **247**, 100–18. doi: [10.1016/j.chemgeo.2007.10.003](https://doi.org/10.1016/j.chemgeo.2007.10.003).
- Zhai MG and Santosh M** (2011) The early Precambrian odyssey of the North China Craton: a synoptic overview. *Gondwana Research* **20**, 6–25. doi: [10.1016/j.gr.2011.02.005](https://doi.org/10.1016/j.gr.2011.02.005).
- Zhang L, Dong CY, Liu SJ, Bai WQ, Ren P and Wan YS** (2016) Early Precambrian magmatism and metamorphism in Ural Mountain area, North China Craton: SHRIMP U-Pb zircon dating and rock geochemical study. *Geological Review* **62**, 1419–38 (in Chinese with English abstract).
- Zhang W and Hu Z** (2020) Estimation of isotopic reference values for pure materials and geological reference materials. *Atomic Spectroscopy* **41**, 93–102.
- Zhang ZQ and Ye XJ** (1987) Mass-spectrometric isotope dilution analysis of REE and precise measurement of $^{143}\text{Nd}/^{144}\text{Nd}$ ratios. *Bulletin of the Institute of Geology, Chinese Academy of Geological Sciences* **1**, 108–28 (in Chinese with English abstract).
- Zhao GC, Cawood PA, Wilde SA and Sun M** (2002) Review of global 2.1–1.8 Ga orogens: implications for a pre-Rodinia supercontinent. *Earth-Science Reviews* **59**, 125–62. doi: [10.1016/S0012-8252\(02\)00073-9](https://doi.org/10.1016/S0012-8252(02)00073-9).
- Zhao GC, Sun M, Wilde SA and Li SZ** (2005) Late Archean to Paleoproterozoic evolution of the North China Craton: key issues revisited. *Precambrian Research* **136**, 177–202. doi: [10.1016/j.precamres.2004.10.002](https://doi.org/10.1016/j.precamres.2004.10.002).
- Zhao GC, Wilde SA, Cawood PA and Sun M** (2001) Archean blocks and their boundaries in the North China Craton: lithological, geochemical, structural and P–T path constraints and tectonic evolution. *Precambrian Research* **107**, 45–73. doi: [10.1016/S0301-9268\(00\)00154-6](https://doi.org/10.1016/S0301-9268(00)00154-6).